Dome patterns in pelagic size spectra reveal strong trophic cascades

Axel G. Rossberg,[1,2,3,*] Ursula Gaedke,[4] and Pavel Kratina[1]

[1]*School of Biological and Chemical Sciences, Queen Mary University of London, Mile End Rd, London E1 4NS, UK*

[2]*Centre for Environment, Fisheries and Aquaculture Science (Cefas), Pakefield Rd, Lowestoft NR33 0HT, UK*

[3]*International Initiative for Theoretical Ecology, Unit 10, 317 Essex Road, London N1 2EE, UK - http://iite.info*

[4]*Department of Ecology and Ecosystem Modeling, Institute for Biochemistry and Biology, University of Potsdam, Am Neuen Palais 10, 14469 Potsdam, Germany*

(Dated: 29 August 2019)

Abstract

In ecological communities, especially the pelagic zones of aquatic ecosystems, certain body-size ranges are often over-represented compared to others. Community size spectra, the distributions of community biomass over the logarithmic body-mass axis, tend to exhibit regularly spaced local maxima, called "domes", separated by steep troughs. Contrasting established theory, we explain these dome patterns as manifestations of top-down trophic cascades along aquatic food chains. Compiling high quality size spectrum data and comparing these with a size-spectrum model introduced in this study, we test this theory and develop a detailed picture of the mechanisms by which bottom-up and top-down effects interact to generate dome patterns. Results imply that strong top-down trophic cascades are common in freshwater communities, much more than hitherto demonstrated, and may arise in nutrient rich marine systems as well. Transferring insights from the general theory of non-linear pattern formation to domes patterns, we provide new interpretations of past lake-manipulation experiments.

* Corresponding author: axel@rossberg.net

This is a pre-print of an article published in Nature Communications. The final authenticated version is available online at: https://doi.org/10.1038/s41467-019-12289-0

INTRODUCTION

Size spectra and food chains belong to the many concepts ecologists have invoked in order to understand structure and dynamics of complex ecological communities. The common conceptualisation of communities as simple *food chains*[1–4] formed by groups of organisms assigned to discrete trophic levels predicts existence of *top-down trophic cascades*[2–7], where pressures on top predators propagate to lower trophic levels, leading to alternating increases and decreases of biomass along the food chain. Such cascades are well documented[8]. Their strengths, however, vary considerably between study systems[6]. Differences in nutrient supply might contribute to this variation, in particular in pelagic ecosystems, where nutrients are known to play a crucial ecological role. This idea, however, has remained controversial. A review from 2010 presented evidence in support of three competing hypotheses[9]: that pelagic cascades are strongest at the highest nutrient concentrations, that they are strongest at intermediate nutrient concentrations, and that cascade strength is largely independent of nutrient availability and primary production. More recent reviews[10,11] do not see nutrient supply amongst the factors affecting cascade strengths. This is surprising, since increasingly sophisticated food-chain models have predicted stronger cascades for more productive systems[4,12,13]. Does this discrepancy indicate inherent limitations of food-chain theory?

An alternative way of looking at the structure of an ecological community is its *size spectrum*, the distribution of community biomass over the logarithmic body size axis[18–22], which can span a factor $> 10^{14}$ in body mass (Fig. 1a). Size-spectrum theory underlies the use of size-based indicators in status assessments of aquatic ecosystems[23]. In pelagic size spectra one often observes distinct body-size ranges of high biomass density[24], known as *domes*[25], and depleted *troughs* between domes (Fig. 1a,b). The question what causes these domes remains subject of ongoing speculation[26–30], but the most common explanation invoked in recent empirical literature[15,31,32] and reviews[19,21] implies that the domes represent subsequent members of the aquatic food chain[25]. The dome structure arises through a *bottom-up cascade*, where the position and height of each dome is controlled by that to its

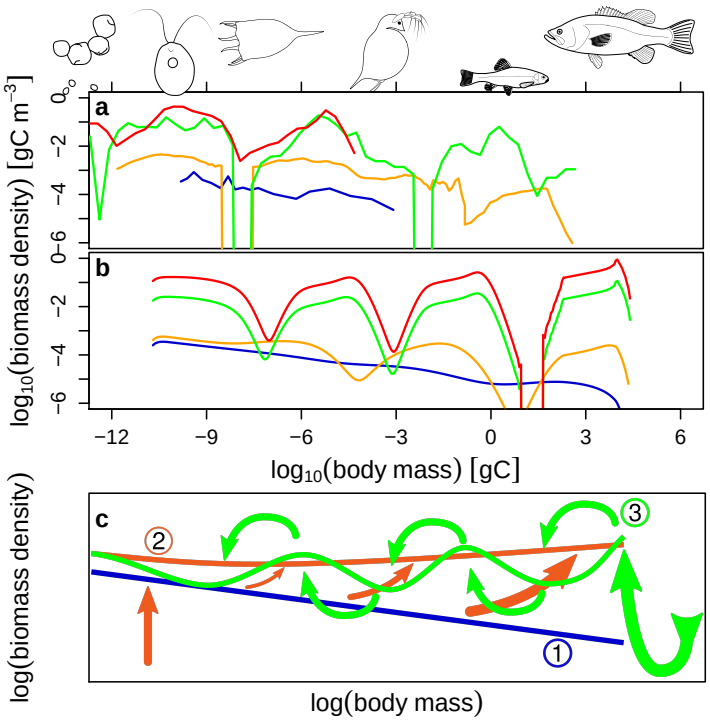

FIG. 1. **Illustration of dome formation in size spectra.** Empirical size spectra in panel **a** are, in order of increasing nutrient enrichment (lowest to highest line), from the North Pacific[14] (blue), Lake Superior[15] (orange), Lake Ontario[16] (green), and Lake Müggelsee[17] (red). See Methods for the representation of size spectra used. Comparable simulation data in panel **b** are steady states of the Species Size Spectrum Model (SSSM) with varying eutrophication parameter x (lowest to highest line; blue: $x = 1$, orange: $10^{0.2} = 1.58$, green: $10^{1.6} = 39.8$, red: $10^{2.4} = 251$). Panel **c** illustrates the causal chain generating domes in the SSSM. ① At low nutrient supply, the size-spectrum forms an approximate straight line on double-logarithmic axes (blue line). ② Increasing nutrient supply increases abundance of primary producers, and, through bottom-up trophic amplification, induces an upward-bending of the entire size-spectrum (orange line and arrows). ③ As a result, consumers become more satiated and more abundant relative to their resources, which both acts to amplify top-down cascades[4,13]. Low predation mortality of the top predators induces such a cascade. This leads to formation of several domes along the size spectrum (green line and arrows).

left on the size axis[33,34]. For the left-most dome, another explanation would be required.

Here we provide evidence for an alternative interpretation of domes, which, by combining ideas from food-chain and size-spectrum theory, resolves open questions pertinent to both.

We demonstrate that domes are manifestations of top-down trophic cascades, enhanced by eutrophication (Fig. 1c). From the size-spectrum perspective, the result is a pronounced *periodic modulation* of the density of community biomass (large domes, deep troughs) along the logarithmic body size axis that becomes weaker with lower nutrient availability[35] (smaller domes, shallower troughs) and, in the oligotrophic open ocean, might disappear entirely[14,18] (Fig. 1a,b). At intermediate to high nutrient concentrations, however, non-linear effects can lead to deviations from classical food-chain theory in how size-spectra respond to pressures.

Self-organised periodic (i.e. regularly spaced) patterns, such as stripe patterns on animal skins, are a common natural phenomenon. It has long been speculated that such structures can arise not only in physical space but also in abstract spaces, for example when competition generates patterns in ecological trait spaces[36–43]. However, any attempt to explain periodic patterns in nature must be mindful that general mathematical principles alone already predict periodic patterns as a common phenomenon[44]. Indeed, size-spectrum models can generate modulations through a variety of mechanisms[26–29,45]. Echoing a similar conundrum surrounding regularities in planetary orbits[46], determination of how domes arise in nature therefore requires more detailed agreement between data and model than the mere fact that modulations are found. Insufficient demonstration of such agreement for existing process-based models is the reason why the dome pattern remains enigmatic. The need for detailed comparisons also limits what can be learned from minimal food-chain[4,13] or size-spectrum[26,47] models, despite their important role in illuminating basic mechanisms. Our comparison of model and data therefore considers specific patterns in the responses of size spectra and domes to nutrient enrichment.

Our working model, the non-linear Species Size Spectrum Model, is designed to incorporate crucial elements of ecological realism while preserving mathematical simplicity and computational efficiency. This permits us to overcome limitations of earlier modelling approaches[20–22]. Using this model, we identify the mechanisms controlling the dependence of dome structure on nutrients, thus permitting us to delineate the conditions required for these patterns to arise.

RESULTS

The non-linear Species Size Spectrum Model

We found that a generalisation of the linear Species Size-Spectrum Model (SSSM)[29] to a full, non-linear model is capable of reproducing the observed phenomenology of domes (Fig. 1). The SSSM belongs to a family of similar models[28,48,49] going back to the Fish Community Size-Resolved Model[50–52]. Structure and motivation of the SSSM are best understood in the wider context of size-spectrum theory[20].

In the simplest dynamic size-spectrum models, individuals interacting in a community are distinguished only by their body masses[26,27,47]. New individuals are added at a constant rate or abundance at the lower end of the modelled size range. Individuals then grow by feeding on each other (or on small planktonic organisms that are not explicitly modelled) and converting the biomass of their prey into their own—at some given efficiency. These feeding interactions lead to corresponding predation mortality. The strength of feeding interactions is controlled by a predator-prey mass-ratio window function; it depends only on the body masses of predator and prey. Life-history parameters and physiological rates scale allometrically with body size. The resulting size-spectrum dynamics is described by a flux-divergence equation for the density of individuals along the size axis, known as the McKendrick von Foerster Equation[26,53].

More advanced models[20,50] distinguish indiviudals not only by body mass but also by species identity, permitting these models to give a full account of the reproductive cycle. Each species has an associated maturation body mass, above which indiviuals invest a large proportion of food intake into reproduction rather than ontogenetic growth. The reproductive investment determines the rate at which individuals of each species are added at the lower end of the modelled size range of that species. In this model class, community dynamics are described by a system of coupled McKendrick von Foerster Equations, one for each species. Any species' population biomass can grow or decline, and species experiencing low food availability and high predation mortality throughout their life cycles can go extinct.

Indeed, when modelling feeding interactions as depending only on the body masses of predators and prey, very few species coexist in these models[54]. A natural way to overcome this limitation is to acknowledge that, while body mass is an important trait affecting feeding

interactions, the combined influence of all other traits can be even stronger[55,56]. In models this is implemented by either equipping species with abstract secondary traits[56,57] (usually assigned at random) that affect the strength of feeding interactions[58,59], or by directly multiplying the size-dependent interaction strength with a non-negative factor sampled at random for each species pair[50,52]. Both approaches lead to food-web models in which species of similar size can have very different prey and predators, implying reduced competition and a lower likelihood of competitive exclusion. While in these models many species can coexist, the original simplicity of the size-spectrum approach is lost. Species-rich models of this type become computationally expensive.

An important observation made studying such models is that the *community size spectrum*, obtained by adding the size spectra of all modelled species, is dominated for any given size class by species with maturation body sizes close to this size class[50]—consistent with analytic theory[29,53] and field data[60,61]. Structure and dynamics of community size spectra over large size ranges are therefore determined predominantly by variations in the population biomasses of species of different sizes, rather than by variations in intraspecific size structure[61,62].

The SSSM builds on this observation. Using an analytic technique called quasi-neutral approximation[63] (QNA), the species-level McKendrick von Foerster Equations are replaced by a system of coupled ordinary differential equations for the dynamics of the species' population biomasses. The QNA is a powerful technique that permits us to retain implicitly descriptions of individual-level processes. In particular, the SSSM captures the Type II functional responses of individuals to food availability from the underlying size-structured food-web model[50], and so the possibility of consumer satiation.

Because the SSSM aims to describe species-rich communities in a computationally efficient way, species are thought of as being grouped into narrow maturation body mass classes, revealing the distribution of community biomass over the logarithmic maturation body mass axis: the *species size spectrum*. The SSSM primarily models the dynamics of this species size spectrum. From this, the community size spectrum is reconstructed following the QNA methodology. However, as a results of lumping species into maturation body mass classes, their differentiation by secondary traits, found to be essential for food-web models of size-structured populations, gets lost. To counteract the resulting artificial competitive exclusion dynamics for species of similar size, the SSSM contains a phenomenological correction term[29],

which accounts for differentiation of species by secondary traits. The structure of this term is similar to the intraspecific competition terms included in Lotka-Volterra models for niche differentiation along a single trait axis[39], but in the SSSM it is constructed such as to avoid unaccounted biomass losses.

Rather than explicitly distinguishing between primary producers and consumers in size spectra, the SSSM imposes a lower boundary condition that fixes the abundances of the smallest species modelled. Nutrient enrichment is modelled by scaling these abundances by a eutrophication parameter x, assumed to be proportional to chlorophyll-a concentration. Model equations are listed in Supplementary Note 1 together with a detailed discussion, including our correction to account for secondary traits. Details of simulation methods are described in Supplementary Note 3. The code we used to simulate the SSSM is provided as Supplementary Software 1.

Basic model behaviour

Model simulations with an ecologically plausible parameterization (Supplementary Note 2) demonstrate that nutrient enrichment and the resulting increases in x and overall community biomass do indeed result in strong dome formation (Fig. 1b).

As a simple demonstration that dome formation in this model is governed by a top-down cascading effect, we removed species from two domes at opposite ends of the size spectrum. First, we simulated harvesting of species from the dome with the largest body sizes, by increasing their mortality. This substantially reduced the size-spectrum modulation along the entire body size axis (Fig. 2a), as expected for a top-down cascade. If the domes would represent subsequent members of a food chain, the naive expectation would be that release from predation allows the intermediate dome to rise when the right-most dome is suppressed, but this is not what we found in simulations.

Second, we harvested species from the dome at the smallest body size. This removed that dome, but had little effect on the modulation of rest of the size spectrum (Fig. 2b, red dashes). The effect it had on larger-bodied individuals is explained by the overall removal of biomass from the system; it is identical to that resulting from a reduction of the eutrophication parameter from $x = 1.58$ to 1.38 (Fig. 2b, blue dots).

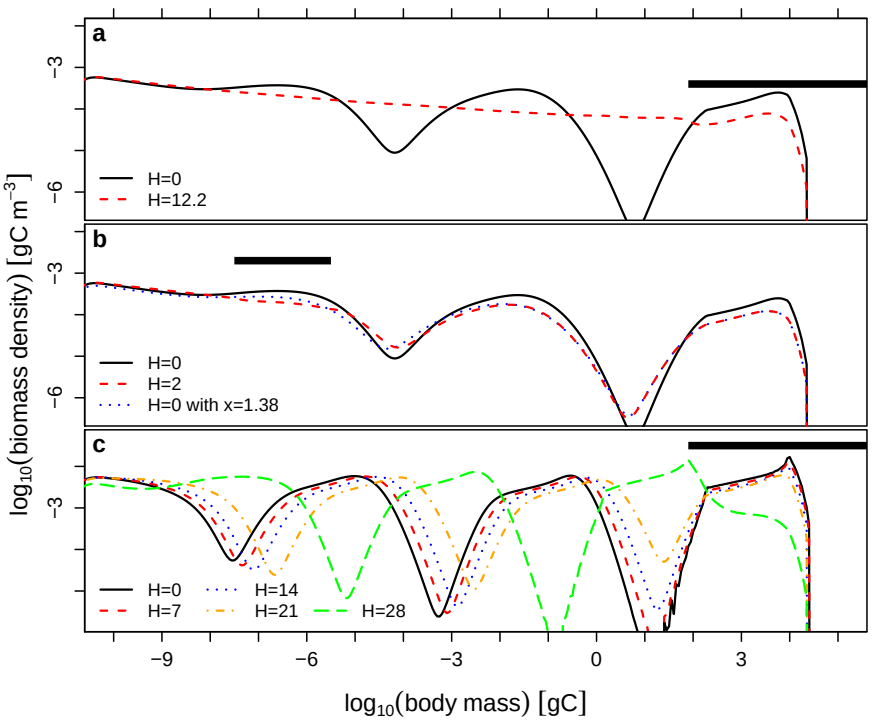

FIG. 2. **Demonstration of top-down and bottom-up effects in SSSM simulations.** Species with body mass at first maturation m_* in the ranges indicated by the horizontal bars (panels **a**,**c**: $m_* \geq 10^{-1.9}\,\mathrm{gC}$; panel **b**: $10^{-7.5}\,\mathrm{gC} \leq m_* \leq 10^{-5.5}\,\mathrm{gC}$) are harvested at an allometrically scaled rate $(m_*/\mathrm{gC})^{-1/4}H$ with H as given in the legend. Panels **a** and **b** show community size spectra for moderate nutrient supply (eutrophication parameter $x = 10^{0.2} = 1.58$). The dome structure can be top-down controlled (**a**) but not bottom-up controlled (**b**). In panel **c**, nutrient supply is higher ($x = 10$) and dome size controlled through inherent non-linear regulation[64] rather than cascading pressures. Contrasting panel **a**, top-down forcing H in panel **c** therefore barely affects the height of the size-spectrum mode near $10^{-5}\,\mathrm{gC}$ body mass; only the position of the mode shifts.

Comparison with data

In addition to generating domes in process-based simulations, our model reproduces much of the rich phenomenology associated with nutrient enrichment in pelagic ecosystems, providing further strong support for the theory. To demonstrate this, we compiled 25 high-quality size spectrum data sets from the empirical literature. We only included data sets spanning at least six orders of magnitude in body mass that provided volumetric biomass density measures and where trophic status has been quantified as total phosphorus (TP)

or chlorophyll-a concentration (which we then expressed as TP using a published regression). To allow quantitative comparison of size spectra across studies, we expressed them in units of gram carbon[65] and as biomass densities along the ln(body mass)-axis[14,29]. Visual inspection of this data (Fig. 1a, Supplementary Note 4) confirms previous reports[65] that, on double-logarithm axes, pelagic size spectra exhibit a linear relation that tends to be overlayed with a secondary structure of uniformly spaced domes. To quantify these features, we fitted both empirical and simulated size spectra to a combination of a linear relation and sinusoidal modulation of the form

$$\log_{10}(\text{biomass density}) = S \log_{10}\left(\frac{\text{body mass}}{1\,\mu\text{gC}}\right) + B_0 + A \sin\left[\frac{2\pi \log_{10}(\text{body mass})}{D} - P\right]. \quad (1)$$

The parameter S, representing the overall slope of the size spectrum, indicates to what extent community biomass is dominated by small organisms ($S < 0$) or large organisms ($S > 0$). Sheldon's hypothesis[18], that biomass is roughly equally distributed over all logarithmic body size classes, corresponds to $S = 0$. The parameter B_0 is the intercept at 1 μgC; it corresponds approximately to the logarithmic biomass of organisms in the size range of herbivorous crustaceans[60]. $A \geq 0$ is the amplitude of modulations. For perfectly sinusoidal dome patterns, 10^{2A} would be the ratio between the biomasses of organisms in the size classes at the peak of domes and on the bottom of neighbouring troughs. Because of deviations from the sinusoidal form, however the actual ratio tends to be larger. The parameter $D \geq 0$ quantifies the separation of domes on the one $\log_{10}$ body mass axis; the body mass ratio of organisms occupying neighbouring domes is 10^D. The parameter P controls the phase of modulations. It shifts the position of domes along the size axis. Below we do not consider it, because its direct comparison across data sets is difficult when D is not fixed. To avoid overparameterization, Eq. (1) does not consider the theoretical possibility of increases or decreases of modulation amplitude along the size axis.

Both empirical and model size spectra occasionally contain gaps, i.e. body size ranges without detectable biomass[65–67] (Fig. 1a,b). We used non-linear median regression to fit Eq. [1], which allowed us to represent these gaps by arbitrary, numerically small biomass densities without biasing the fits. In Supplementary Note 4 we present graphs of all 25 data sets and corresponding fits.

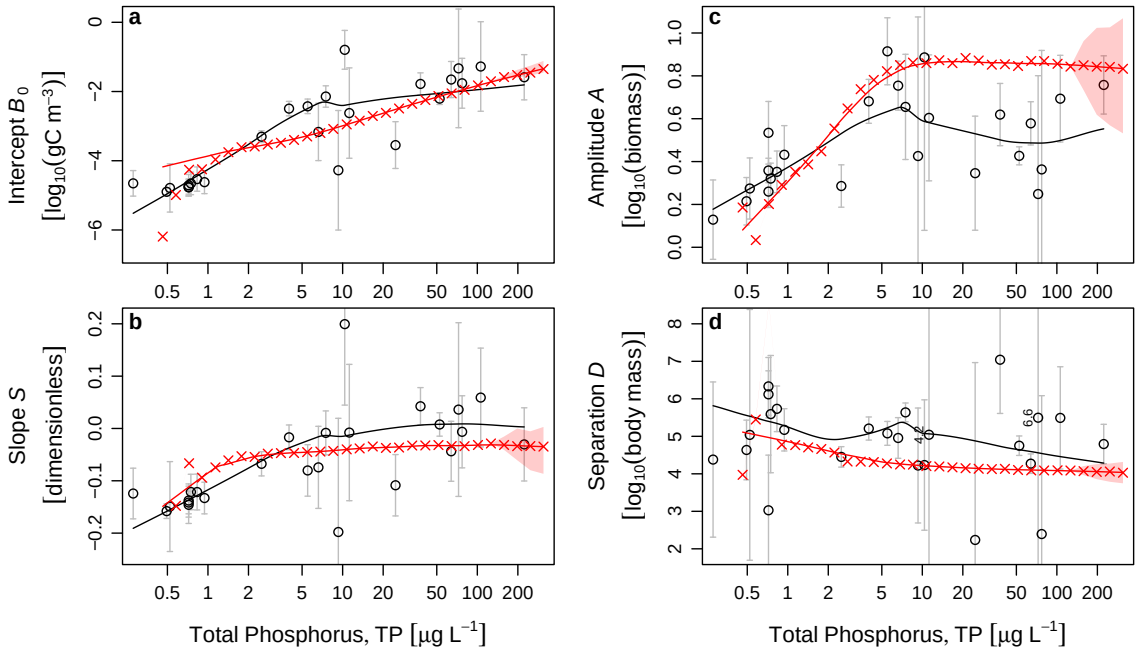

FIG. 3. **Dependence of community size structure on nutrient enrichment.** The four panels quantify intercept B_0 (at $1\,\mu$gC) and slope S of size spectra, the amplitude A of domes and their separation D on the $\log_{10}$-body mass axis, as defined through Eq. [1]. Empirical data (black circles, $\pm$s.e.) and medians over 100 simulation snapshots (red crosses, 1st to 3rd quartile ranges are shaded in pink when the model exhibits steady-state dynamics, see S3 for details). Model runs are for eutrophication parameter $x = 10^{-0.1}$, $10^{0.0}$, $10^{0.1}$, ..., $10^{2.8}$, assuming chlorophyll-*a* concentrations $0.2\,x\,\mu\mathrm{gL}^{-1}$ and converting to TP (Methods). Lines are weighted LOESS smothers. Weighted linear regressions (S5) reveal statistically significant ($p \leq 0.01$, two-sided) dependencies on $\log(\mathrm{TP})$ for empirical intercepts B_0, slopes S, and dome amplitudes A, and a weak but statistically significant ($p = 0.042$) decreases of dome separation D with $\log(\mathrm{TP})$. In cases where error bars extend across graphs, numerical s.e. are written next to data points, thus indicating high ambiguity of the underlying data. Because we weighted empirical data according to inverse squared s.e. in all analyses, these high s.e. data sets contribute less to analyses than, e.g., the highly consistent and accurate measurements for Lake Superior (TP = 2.5) or Lake Constance (TP = 52.5).

Our data comprise a wide range of ecosystems differing in respect to latitude, size and depth, which affect phenomena not modelled in the SSSM, such as prey defence and allochthonous inputs. To validate the SSSM, we therefore do not attempt a quantitative fit to data but constraint ourselves to the objectives of Pattern-Oriented Modelling[68]. That

is, we aim to reproduce qualitative patterns in the empirical responses of the size-spectrum characteristics B_0, S, A, and D to enrichment, and the order of magnitude of these effects. As shown in Fig. 3, the SSSM reproduces well the overall increase in system biomass with enrichment[65] (Fig. 3a). Also in good agreement with observations, enrichment in the model leads to an increasing (less negative) size-spectrum slope[35] S, with the increase becoming less pronounced at higher nutrient levels (Fig. 3b). Importantly, both data[35] and model follow our theoretical expectation (Fig. 1c) that size-spectrum modulations become stronger with enrichment (Fig. 3c). At low nutrient concentrations and resulting small modulation amplitudes, the separation between domes D is ill-defined for both data and model. Once pronounced dome patterns arise, data and model agree in that the separation between domes D is not much affected by trophic status (Fig. 3d, Supplementary Note 7). Thus, all major patterns in the data are reproduced by the SSSM, validating it as a good description of pelagic size spectra.

Mechanisms

As is common in the study of self-organised periodic patterns[44,69], key insights into the mechanisms driving dome formation in size spectra can be gained from studying the linear response of the system to small perturbations. From a previous mathematical analysis[29] it is known that pelagic size spectra exhibit a superposition of three mathematically distinct linear responses to pressure on a single body size class (Fig. 4, Methods, Supplementary Note 6): (i) the top-down cascade, modulating the size spectrum towards lower body size classes[26,28], i.e. leading to alternating enhancement and depletion of biomass along the size axis; (ii) a modulated bottom-up cascade[25,28,33]; and (iii) the conventional, unmodulated bottom-up effect, consistently either enhancing or depleting the biomasses of all larger bodied species. Depending on system parameters, the two modulated responses can be either amplifying or attenuating (in terms of proportional changes in abundance) as they propagate away from the pressure on the size axis[29] (Fig. 4). The conventional bottom-up effect always increases as it travels up the size axis[29], a phenomenon called trophic amplification[70,71].

Dome formation in the SSSM corresponds to a transition from attenuating to amplifying top-down cascades with increasing enrichment, as we demonstrate in a mathematical analy-

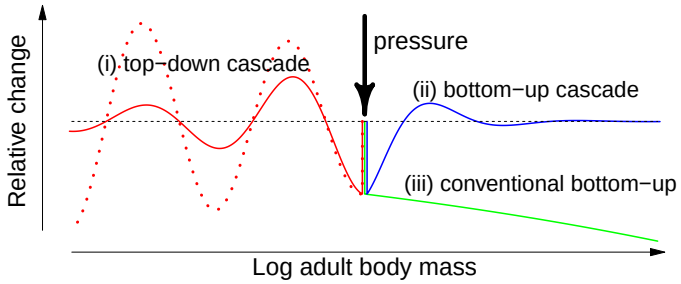

FIG. 4. **The three main distinct responses of size spectra to size-specific pressures.** When species of a specific body-size class are continuously removed from the community (thick arrow), theory predicts (i) a top-down modulation of population abundances towards smaller body-size classes, which may be either attenuating (solid red line) or amplifying (dotted red line); (ii) a bottom-up cascade in the reverse direction (blue); and (iii) an amplifying conventional bottom-up effect (green). Depending on the size class at which the pressure is applied, not all of these effects may unfold. The horizontal dashed line represents the pressure-free state. We find that domes emerge when the top-down cascade becomes amplifying towards smaller body sizes.

sis of the mechanisms at work in Supplementary Note 7. The analysis identifies two distinct mechanisms driving this transition. The first depends on the fact that, due to trophic amplification, the size spectrum slope S increases with enrichment (Fig. 3b). Because consumers tend to be larger than their resources, this increases the abundance of consumers relative to their resources in enriched systems. As a result, a given proportional change in consumer abundance can affect a larger proportional change in resource abundances. The second mechanism is driven by the overall increase of community biomass in enriched systems. As detailed in S7, this leads to partial satiation of consumers and reduces their ability to control their resources, because (i) their food intake rate becomes less dependent on resource abundance and, (ii) resources of satiated consumers experiences a safety-in-numbers effect[72]. Both enhance top-down cascades, as is the case in simple mathematical models of infinite[13] and finite[4] food chains.

It should be noted that the top-down and bottom-up terminology above refers only to the direction of propagation of effects in size spectra. At the food-web level, the underlying processes can be more complicated[29,73,74]. This may explain why, despite providing some indications for top-down cascades[73,74], empirical studies of feeding interactions in size spectra did not fully reveal the nature of dome formation.

Generic arguments developed in the study of self-organised periodic modulation patterns in physics[44,69] imply that, for system parameters far beyond the onset of modulations, the phase of modulation patterns still easily responds to pressures, but not the amplitude. Instead, the modulation amplitude is controlled by inherent non-linear regulation[64,69]. For size spectra, this means that harvesting biomass from one dome does not affect the height of other domes (relative to neighbouring troughs), only their positions along the log(body mass) axis. This could explain why experimental manipulations of the top trophic levels in pelagic communities sometimes do not comply with predictions from simple food-chain theory[2]; often producing pronounced changes in mean zooplankton body size rather than in total zooplankton biomass[2,3]. We demonstrate this effect in Fig. 2c. This sensitivity of dome positions to pressures might also lead to a tendency for domes to form in biologically favoured size ranges, for which there is some empirical evidence[24].

DISCUSSION

A mechanistic explanation

Above, we have explained dome formation as a consequence of nutrient enrichment in three complementary ways[75]: first, by obtaining the empirical relation between dome amplitude and nutrient concentration directly from observation data (Fig. 1a; black circles in Fig. 3c); second, by simulating a process-based model, which demonstrates that individual-level processes lead to dome formation with increasing primary production (Fig. 1b; red crosses in Fig. 3c), and; third, through a mathematical analysis of this model, which reveals step-by-step the causal chain leading from enhanced primary production to the onset of dome formation in a transition from attenuating to amplifying top-down cascades (Fig. 1c; Supplementary Note 7). The present work thus adds to the small number of cases in community ecology where an analytically tractable, process-based model semi-quantitatively explains a rich empirical phenomenology[76–78]. This became possible not only by the judicious construction of our model from simple components (Supplementary Note 1), but also by developing mathematical methods that allowed us to analyse the model despite its complexity (Methods, Supplementary Notes 6 & 7).

The mechanistic analysis permits us to address questions regarding the generality of the process of dome formation. For example, one might ask to what extent dome formation is affected by life-history parameters such as the relative sizes of new offspring, individuals at first maturation, and the largest adults of a species—especially since these proportions vary considerably among species and along the size gradient. Our analysis suggests this dependence is weak: these proportions do not enter the expressions that control the transition to dome formation (Supplementary Note 7). The approximate analytic expression that we derive for the distance D between domes along the logarithmic body mass axis [Eq. (17) of Supplementary Note 7] depends only on two parameters characterising the typical range of body-mass ratios between individual predators and their prey, and an allometric scaling exponent.

Another implication of the mechanistic theory follows from the fact that it makes heavy use of the assumption that predators feed on living prey smaller than themselves. The mechanisms identified are unlikely to operate effectively in food webs that are not as

strongly size structured as pelagic communities. In benthic communities size structure is less pronounced[79]. One can therefore plausibly expect that the dome patterns found in benthic size spectra[80,81] are controlled by different kinds of mechanisms[81,82] and thus respond differently to enrichment than those found in pelagic communities.

Our explanation of dome formation as a transition from attenuating to amplifying top-down cascades is consistent with the conclusion of an earlier meta-analysis that top-down cascades tend to be attenuating in marine pelagic systems but have no such general tendency in the nutrient richer lake pelagic communities[6]. As explained above, the general theory of pattern formation suggests that far beyond the onset of dome formation the dome amplitude is controlled by inherent non-linear regulation[64,69], rather than by the amplitudes of neighbouring domes. When top-down cascades are amplifying in a linear model, as we find for nutrient rich pelagic systems, non-linear effects thus constrain the maximum height that domes eventually attain[64]. This explains why, on average, trophic cascades observed in lake pelagic communities are neither amplifying nor attenuating[6].

Our analytic calculations (Supplementary Note 7) constrain the transition point from attenuating to amplifying cascades to the range $1 < x < 8$ for the model's eutrophication parameter, corresponding to $0.6\mu\text{gL}^{-1} < \text{TP} < 4.4\mu\text{gL}^{-1}$ or chlorophyll-a concentrations in the range 0.2-1.6μgL^{-1}, with lower values preferred when size-spectra span longer body-size ranges. Coastal marine waters often lie in this transition range (which is below levels where harmful algal blooms tend to occur[83,84]). On this basis, we predict the occurrence of dome patterns in nutrient rich coastal marine waters. Climate warming can increase coastal surface nutrient concentrations further[71], thus intensifying this effect, with potential implications for marine ecosystem management. However, we caution that the transition from attenuating to amplifying top-down cascades does not result in a sharp qualitative transition in observed size spectra. For example, the cascade in the unperturbed model size spectrum for $x = 1.58$ (Fig. 2a, black line) is still attenuating (compared to neighbouring domes, the right trough is deeper than the left), yet it already exhibits a clear dome structure.

The analytic calculations also reveal why models simpler than the SSSM would struggle to convincingly explain dome formation. All details of the SSSM that distinguish it from previous, simpler size-spectrum models have a role to play in reproducing and explaining the phenomenology we report. Size-spectrum models that do not distinguish individuals by maturation body mass[26,27,47] are unable to represent in their steady state the gaps ob-

served in size spectra[65,66], because there is no biological mechanism to generate individuals of body sizes larger than the size class of a gap. Models without any representation of intraspecific size structure[34] would, amongst others[29], overestimate the magnitude of domes and the prevalence of gaps. Models representing communities as food chains[13] rather than as continua of species cannot represent shifts in the positions of domes in response to pressures[69], as seen in Fig. 2c. Models without representations of consumer satiation[26,27] omit a model component that is essential for the transition to amplifying cascades. Models that include non-linear stock-recruitment relationships in addition to[28] (rather than implied by[52]) density-dependent feeding interactions are unlikely to generate amplifying top-down cascades or bottom-up amplification, because they tend to overestimate the strength of inherent regulation of population size. Models that explicitly evaluate food webs of size-structured populations without imposing artificial[20] limits to recruitment[50,52], i.e. the type of models that the SSSM approximates, tend to be computationally too expensive for simulations of species-rich communities over size ranges as large as studied here. The SSSM's demonstrated ability to describe high-level phenomena in pelagic ecosystems over a wide range of conditions suggests future applications in diverse areas such as the testing of ecological indicators, development of management strategies, or ecological forecasting.

The significance of our results lies not only in the characterisation of dome patterns or top-down cascades, but crucially in the identifications of the former as manifestations of the latter. This became possible by understanding dome formation as part of a wider scenario of community change with increasing enrichment (Fig. 3). In particular, the results speak against the widely cited idea that domes represent bottom-up cascades[25,33,34]. While bottom-up cascades have indeed been demonstrated in the SSSM and similar models[28,29], our mathematical analysis (Supplementary Notes 6 & 7) shows that these cascades get damped by increasing enrichment, opposite to the observed pattern (Fig. 3). Based on the classical theory, we had also expected that the flattening of the dome with smallest body size in model simulations (Fig. 2b) would similarly reduce modulations along the entire size-spectrum, which was not the case.

Relation to detailed empirical accounts

When comparing our theory with detailed observations in specific ecological communities, it must be kept in mind that any size-spectrum model is a simplified high-level description. It relates to low-level descriptions in terms of populations and their interaction networks in an analogous manner as a macroscopic description of sound waves in an air-filled chamber relates to a microscopic description of the air in terms of freely moving and occasionally colliding molecules. Concepts that are central to a high-level description (domes, sound waves) are unnecessary or even meaningless for a full description and explanation of dynamics at the lower level. When a detailed low-level description is available, one can, *a posteriori* reconstruct the macroscopic phenomenon (modulation of community biomass along the size axis for domes, density waves for sound), but this does not add information to that already provided at the lower level. To the contrary, since high-level descriptions are generally approximations, their juxtaposition with corresponding low-level descriptions will necessarily reveal inaccuracies.

Such juxtapositions, relating the populations and interactions of species and functional groups to the resulting size spectra, are available, for example, for Lake Constance and Lake Müggelsee[17,60,61,73,85]. One particular effect that size-spectrum models cannot capture, which was identified in these studies, are changes in the distributions of traits other than size[86]. Yet, such changes must be expected as part of a re-organisation of community structure, e.g., in response to nutrient enrichment. For example, it has been observed that the size range covered by carnivorous zooplankton may change[17,60] and less edible phytoplankton may pile up in certain size classes of the autotrophic size range, so reducing the flow of biomass towards larger consumers[17]. Conversely, particularly efficient and competitive consumers such as daphnids may obtain biomasses above the average zooplankton due to their ability to exploit relatively small and thus highly productive prey[60,73].

Such low-level descriptions and the higher degree of detail they provide do not, however, invalidate high-level descriptions, e.g., in terms of size-spectrum models. Low-level descriptions tend to be system specific and would struggle, for example, to provide simple explanations of trends seen across systems, such as those documented in Fig. 3—while the SSSM achieves just this.

Conclusion

Along multiple lines of evidence we have demonstrated that the dome patterns found in pelagic size spectra of lakes are likely governed by top-down trophic cascades and moderated by the availability of nutrients. The frequent observation of pronounced dome patterns[15–17,24,34,66,73], where variation in biomass often exceeds a factor 100 (Fig. 1a), therefore suggests that strong top-down cascades are common in freshwater communities. These powerful trophic cascades, generating domes, are active in pelagic systems without any manipulation of top trophic levels[2,3]. Pelagic dome patterns might therefore be the clearest cases yet of self-organised ecological pattern formation in trait space.

The results of this study imply that measurement of the strength of top-down cascades in lakes does not necessarily require experimental manipulations or comparative studies. Cascade strength can be estimated directly from the modulation amplitude of size spectra (Fig. 3c). Application of this idea to the old question of how cascade strength depends on nutrients provides clear evidence for an overall increase of cascade strength with increasing nutrient concentration in both model and data (Fig. 3c) up to around 5-10 μgL^{-1} TP. Beyond this level there might be plateau or even a slight decline in cascade strength with TP. Thus, several of the patterns previously considered[9] appear to be combined. To further clarify the details of this dependence, we call for systematic measurements of size spectra across nutrient enrichment gradients, aided by the accurate automated methods now available[15]. Monitoring of coastal marine size spectra might guide the interpretation of ecosystems changes when domes form unexpectedly.

For bio-manipulation of top predators[2,3], we predict that measurements of size spectra in lakes will, depending on trophic status, reveal responses of the amplitude or the phase of the dome pattern (Fig. 2). Responses to pressures on high-ranking predators will therefore not always follow expectations from simple food-chain theory[2,3], but transfer of pressures to lower trophic levels should generally be expected in the light of the new theory. The general theory of non-linear pattern formation thus provides new mechanistic insights into the structure and dynamics of ecological communities.

I. METHODS

Representation of size spectra

For the purpose of comparison across studies, empirical size spectra are often represented on double-logarithmic axes in the so-called *normalised* form[87,88]: the volume (or areal) density of biomass of organisms measured in each body mass interval considered is divided by the linear width of this interval (of dimension Mass). In the limit in which the width of these intervals goes to zero, this represents the density of a community's biomass (per unit volume) along the linear body mass axis[89]. A disadvantage of this representation is that normalised spectra tend to spread over a wide numerical ranges. Superimposed "dome" modulations are not easily visible.

To overcome this disadvantage while maintaining comparability of spectra across studies, we computed not the density of biomass (per unit volume) along a linear but along a logarithmic body mass axis. Specifically, the natural logarithm of body mass was used, which permits a simple conversion of traditional normalised size spectra to this density-along-the-log-axis form: one just needs to multiply each normalised size spectrum value by the corresponding body mass. To obtain unbiased estimates of the continuous size spectrum from empirical data for discrete size intervals one multiplies with the geometric mean of upper and lower interval boundary[29]. This is the representation used throughout the present study:

$$\text{size spectrum at point } m_i = \frac{B_i m_i}{\Delta m_i}, \tag{2}$$

with m_i denoting the geometric mean of the boundaries of body mass interval i (i.e. the mid point on a log axis), Δm_i its linear width, and B_i the measured biomass volume density of individuals with body mass lying in this interval. Equation [2] is formally equivalent to a known heuristic "denormalisation" procedure for size spectra[14,87,88].

Data sets

Searching for the keywords "size spectrum" and "size-spectrum" in literature databases and following relevant citations, we identified 25 pelagic size-spectrum datasets that satisfied our inclusion criteria (good technical quality, coverage of a 10^6 body-mass range, and

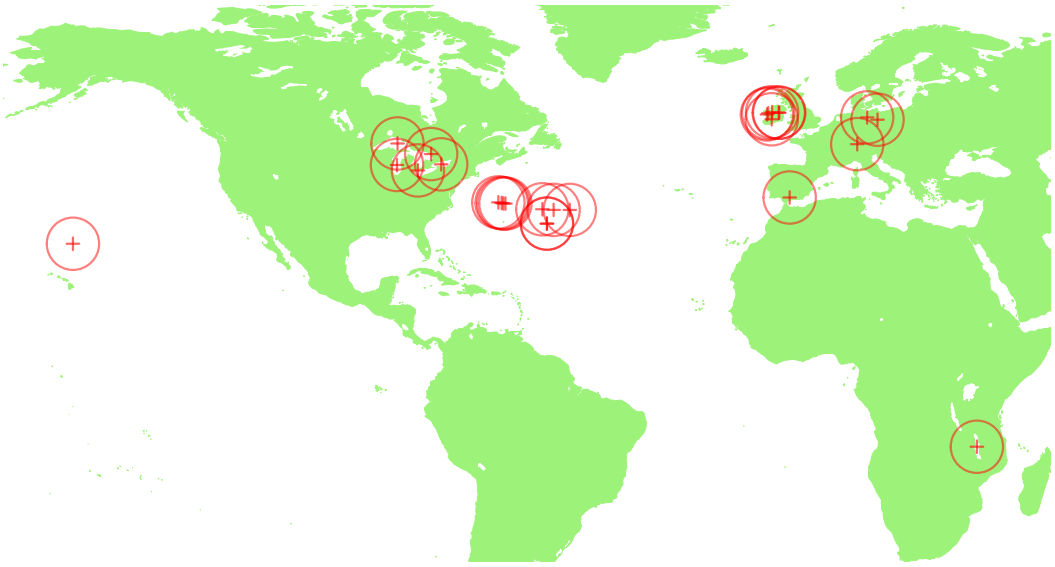

FIG. 5. **Locations of study sites included in analysis**

quantification of trophic status). Except for a data sets from Lake Malawi, all sampling locations lie within the latitudinal band 28°-54°N (Fig. 5).

In some cases, uneven sensitivity of sampling and use of different sampling methods over different size ranges can lead to structures in the data that resemble dome patterns. Occurrence of such artefacts, however, can be recognised by comparing method boundaries along the size axis and dips or discontinuities in spectra, and usually such issues are acknowledged by study authors. We excluded two studies because of such concerns[90,91]. While uneven sampling might also have contributed to some of the unevenness in other spectra (just as any empirical method has potential biases), the fact that we find a clear signal of increasing dome amplitude A with increasing nutrient richness (Fig. 3) in accordance with earlier observations[35] would be hard to explain if sampling artefacts where generally the dominating contribution to size-spectrum modulations.

We converted chlorophyll-a concentrations [Chl-a] to total phosphorus concentrations TP using the relation[92] ["This study (all lakes)" in the source] $\log_{10}[\text{Chl-}a] = -0.455 + 1.026\,\log_{10}(\text{TP})$, i.e. $\log_{10}(\text{TP}) = (\log_{10}[\text{Chl-}a] + 0.455)/1.026$, with [Chl-$a$] and TP given in μgL^{-1}. The conversion was used mostly for marine systems, where nutrients other than phosphorus may be (co-)limiting. The TP values so obtained have therefore purely nominal character as expressions of overall nutrient availability.

The following lists the systems underlying the empirical data in Figs. 1 and 3, together with data sources for size spectra and, if different, sources for TP or [Chl-a] (expressed in μgL^{-1}): North Pacific Central Gyre[14] with[93] [Chl-a] = 0.0945 (corresponding to TP = 0.28); stations Purple 10 ([Chl-a] = 0.17, TP = 0.49), Purple 11 ([Chl-a] = 0.18, TP = 0.52), Yakutat ([Chl-a] = 0.25, TP = 0.72), Nashville ([Chl-a] = 0.25 , TP = 0.72) and Indigo ([Chl-a] = 0.26, TP = 0.75) in the New England Seamounts Area[94] and stations Sargasso 12 ([Chl-a] = 0.25, TP = 0.72), Sargasso 14 ([Chl-a] = 0.29, TP = 0.83), and Sargasso 13 ([Chl-a] = 0.33, TP = 0.94) in the Sargasso Sea[94], where data points below $5 \cdot 10^{-13}$ gC body mass were discarded due to acknowledged methodological artefacts[94]; Lake Superior[15] with[95] TP = 2.5 (average of years 2006 and 2011, numerical data by Peder M. Yurista, priv. comm.); the averaged spectrum of 37 inland lakes in central Ontario[24,65] with median TP = 4[24,65]; Lake Michigan[96] with TP = 5.5[97]; the six Irish lakes[98] Loughs Maumwee (TP = 6.6), Carra (TP = 11.2), Gara (TP = 24.7), Gur (TP = 37.9), Mullagh (TP = 72.6) and Ramor (TP = 77.1, numerical data by Elvira de Eyto, priv. comm.); Lake Ontario[16] with TP = 7.5[95]; Lake Malawi[16] with TP = 9.3[99]; Lake St Clair[35] (average over 14 stations, TP = 10.4); Lake Constance[60] averaged over years 1987-1996 (unpublished data by U.G.) with TP = 52.5[100]; Fuente de Piedra[101] ([Chl-a] = 25[102], TP = 64.0); Arendsee[66] (TP = 106); and Müggelsee[17] averaged over years 1988-1990 (numerical data by U.G., TP = 223). Size-spectrum data were extracted from referenced published graphs if not stated otherwise. When publications contained multiple graphs with size spectra for a given system, we selected the spectra averaging over the longest time interval and the largest number of stations. CSV files of the size-spectra analyzed in this study are included as Supplementary Data 1.

Missing empirical values

Size-spectrum values of zero are sometimes suppressed in empirical data. In published size-spectrum data sets, we therefore identified as a gap any occurrence of a large interval between subsequent reported size-class midpoints. Precisely, any spacing on the log-body-mass axis between subsequent reported size-class midpoints that was over 1.8 times wider than both the previous and the subsequent spacing was considered a gap. Each such gap was filled by a single size-spectrum value of zero at the centre of the gap. All reported values of zero were retained, except for those at the upper end of reported body mass ranges, since

these might be due to insufficient sample volumes. Before taking logarithms, size spectrum values of zero were replaced by 10^{-100} times the smallest reported non-zero value. The thus processed size spectra are included in Supplementary Data 1 as an R object.

Size range used to determine characteristics

For most empirical data sets (84%), the body size range covered does not extend beyond 0.1 gC. For comparability across empirical data sets and between data and simulations, only size-spectrum data up to 0.1 gC were therefore used when fitting Eq. [1] to extract the characteristics B_0, S, A, and D. We stress that this restriction of the size range is a decision about how to characterise the size spectra. It does not imply a statement about what size range is dynamically relevant in either models or reality. The role of the distinction between models and characterisations in the development of ecological theory is discussed in[13].

Non-linear median regression

To fit Eq. [1] to size spectrum data, we used the function `nlrq` from the package `quantreg` (v. 5.36) of the R programming language, v. 3.5.3,[103], which implements an interior point method for non-linear quantile regression[104]. The function requires initial parameter values for a non-linear optimisation routine, which we set to $B_0 = -2.5$, $S = -0.1$, $A = 1$, and all combinations of $D = 4$, 6 and $P = 0$, 0.4π, 0.8π, 1.2π, 1.6π. When different initial values resulted in different fits, the result best satisfying the quantitative optimisation criterion of the fitting method was selected. However, values for dome separation were constrained to the range $D = 2$ – 9, because size spectrum modulations with very small or very large wavelengths were not phenomena of interest to the present analysis. Standard error estimates for the empirical fitting parameters were computed using the jackknife method.

LOESS smoothes

Smoothes in Fig. 3 are first-order LOESS based on the closest 2/3 of data points (1/3 for simulations), weighted by tricubic distance and for empirical data in addition by inverse squared estimated standard error. To improve the robustness of the smoothes, they were

computed using M-estimation with Tukey's biweight using the function `loess` of `R`.

Mathematical analysis

We outline the mathematical methods used to establish the mechanisms driving the transition from attenuating to amplifying top-down cascades in the SSSM. For details see Supplementary Notes 6 & 7.

The standard methods[44] to identify the conditions and driving mechanisms for the formation of self-organised periodic patterns, i.e. spatial modulation of some system property, relies on the computation of the linear growth rate (in time) of small, sinusoidal perturbations of the unmodulated base state of the study system. When modulations grow through time, patterns form. But this method is not applicable here. Because of allometric scaling of physiological rates, the dynamics of small species tend to be much faster than that of large species, so that periodic modulations do not have well-defined linear growth rates (they are not eigenfunctions of the linearized dynamics). The method used here[29] therefore considers instead the static, equilibrium linear response of the system to small, sustained, localised press perturbations. For this, the allometric scaling plays no essential role. Patterns form when the equilibrium response increases with the distance from the perturbation along the size axis. In Supplementary Note 6 we demonstrate for an exactly solvable example that in cases where both methods are applicable they give equivalent results.

In size-spectrum models, the equilibrium response to localised pressures can be decomposed into a sum of sinusoidal responses that, starting from the perturbed size class, grow or decline exponentially along the logarithmic size axis, plus unmodulated exponentially growing or declining components (as in Fig. 4). In addition to these exponential components, the static response may have a localised core residual that declines faster than exponential with the distance from the perturbation[29]. Each component of the sum has a characteristic complex-valued wave number, the real part of which is 2π divided by the wavelength of the sinusoidal modulation, and the imaginary part the rate of exponential growth or decay along the logarithmic size axis.

To determine these wave numbers, one first needs to compute the effective interaction kernel for species along the size spectrum. This function describes the dynamic linear response of species in all size classes to changes in the abundance of species in one given size

class. The interaction kernel thus encapsulates the underlying ecology. The wave numbers of the linear modes of the size spectrum are give by the zeros, in the complex plane, of the analytic continuation of the Fourier transform of this interaction kernel.

While for the SSSM this Fourier transform is a rather complicated mathematical expression, it turns out that at most points in the complex plane just a few terms of this expression (associated with specific ecological phenomena) dominate numerically. Hence, the locations of the zeros can be understood from the properties of just a few terms.

In our mathematical analysis, changes in the interaction kernel due to nutrient enrichment are described by a heuristic modification of the kernel that corresponds to an overall increase in food availability. Using this to study the effects of enrichment on the Fourier transform of the interaction kernel, the mechanisms driving the transition from attenuating to amplifying top-down cascades are then identified.

DATA AVAILABILITY

All data analysed in this study are included in a supplementary information file.

CODE AVAILABILITY

The simulation code used in this study is included in a supplementary information file.

[1] Paine, R. T. Food webs: Linkage, interaction strength and community infrastructure. *J. Anim. Ecol.* **49**, 667–685 (1980).

[2] DeMelo, R., France, R. & McQueen, D. J. Biomanipulation: Hit or myth? *Limnol. Oceanogr.* **37**, 192–207 (1992).

[3] Carpenter, S. R. *et al.* Trophic cascades, nutrients, and lake productivity: Whole-lake experiments. *Ecol. Monogr.* **71**, 163–186 (2001).

[4] Heath, M. R., Speirs, D. C. & Steele, J. H. Understanding patterns and processes in models of trophic cascades. *Ecol. Lett.* **17**, 101–114 (2014).

[5] Barbier, M. & Loreau, M. Pyramids and cascades: A synthesis of food chain functioning and stability. *Ecol. Lett.* **22**, 405–419 (2019).

[6] Shurin, J. B. *et al.* A cross-ecosystem comparison of the strength of trophic cascades. *Ecol. Lett.* **5**, 785–791 (2002).

[7] Jeppesen, E. *et al.* The impact of nutrient state and lake depth on top-down control in the pelagic zone of lakes: A study of 466 lakes from the temperate zone to the Arctic. *Ecosystems* **6**, 313–325 (2003).

[8] Estes, J. A. *et al.* Trophic downgrading of planet Earth. *Science* **333**, 301–306 (2011).

[9] Carpenter, S. R., Cole, J. J., Kitchell, J. F. & Pace, M. L. Trophic cascades in lakes: Lessons and prospects. In Terborgh, J. & Estes, J. A. (eds.) *Trophic Cascades: Predators, Prey, and the Changing Dynamics of Nature*, 55–69 (Island Press, 2010).

[10] Salomon, A. K. *et al.* Key features and context-dependence of fishery-induced trophic cascades. *Conserv. Biol.* **24**, 382–394 (2010).

[11] Piovia-Scott, J., Yang, L. H. & Wright, A. N. Temporal variation in trophic cascades. *Annu. Rev. Ecol. Evol. Syst.* **48**, 281–300 (2017).

[12] Sarnelle, O. Nutrient enrichment and grazer effects on phytoplankton in lakes. *Ecology* **73**, 551–560 (1992).

[13] Rossberg, A. G. *Food Webs and Biodiversity: Foundations, Models, Data* (Wiley, 2013).

[14] Rodriguez, J. & Mullin, M. M. Relation between biomass and body weight of plankton in a steady state oceanic ecosystem. *Limnol. Oceanogr.* **31**, 361–370 (1986).

[15] Yurista, P. M. *et al.* A new look at the Lake Superior biomass size spectrum. *Can. J. Fish. Aquat. Sci.* **71**, 1324–1333 (2014).

[16] Sprules, W. G. Ecological change in Great Lakes communities — a matter of perspective. *Can. J. Fish. Aquat. Sci.* **65**, 1–9 (2008).

[17] Gaedke, U., Seifried, A. & Adrian, R. Biomass size spectra and plankton diversity in a shallow eutrophic lake. *Int. Rev. Hydrobiol.* **89**, 1–20 (2004).

[18] Sheldon, R. W., Prakash, A. & Sutcliffe, W. H., Jr. The size distribution of particles in the ocean. *Limnol. Oceanogr.* **17**, 327–340 (1972).

[19] Sprules, W. G. & Barth, L. E. Surfing the biomass size spectrum: Some remarks on history, theory, and application. *Can J Fish Aquat Sci* **73**, 477–495 (2016).

[20] Andersen, K. H., Jacobsen, N. S. & Farnsworth, K. The theoretical foundations for size spectrum models of fish communities. *Can. J. Fish. Aquat. Sci.* **73**, 575–588 (2015).

[21] Guiet, J., Poggiale, J.-C. & Maury, O. Modelling the community size-spectrum: Recent developments and new directions. *Ecological Modelling* **337**, 4–14 (2016).

[22] Blanchard, J. L., Heneghan, R. F., Everett, J. D., Trebilco, R. & Richardson, A. J. From bacteria to whales: Using functional size spectra to model marine ecosystems. *Trends in Ecology & Evolution* **32**, 174–186 (2017).

[23] Shin, Y.-J., Rochet, M.-J., Jennings, S., Field, J. G. & Gislason, H. Using size-based indicators to evaluate the ecosystem effects of fishing. *ICES J Mar Sci* **62**, 384–396 (2005).

[24] Sprules, W. G., Casselman, J. M. & Shuter, B. J. Size distributions of pelagic particles in lakes. *Can. J. Fish. Aquat. Sci.* **40**, 1761–1769 (1983).

[25] Boudreau, P. R., Dickie, L. M. & Kerr, S. R. Body-size spectra of production and biomass as system-level indicators of ecological dynamics. *J. Theor. Biol.* **152**, 329–339 (1991).

[26] Benoît, E. & Rochet, M.-J. A continuous model of biomass size spectra governed by predation and the effects of fishing on them. *J. Theor. Biol.* **226**, 9–21 (2004).

[27] Law, R., Plank, M. J., James, A. & Blanchard, J. L. Size-spectra dynamics from stochastic predation and growth of individuals. *Ecology* **90**, 802–811 (2009).

[28] Andersen, K. H. & Pedersen, M. Damped trophic cascades driven by fishing in model marine ecosystems. *Proceeding R. Soc. B* **277**, 795–802 (2010).

[29] Rossberg, A. G. A complete analytic theory for structure and dynamics of populations and communities spanning wide ranges in body size. *Adv. Ecol. Res.* **46**, 429–522 (2012).

[30] dos Santos, R. M., Hilbers, J. P. & Hendriks, A. J. Evaluation of models capacity to predict size spectra parameters in ecosystems under stress. *Ecol Indic* **79**, 114–121 (2017).

[31] Quiroga, E., Gerdes, D., Montiel, A., Knust, R. & Jacob, U. Normalized biomass size spectra in high Antarctic macrobenthic communities: Linking trophic position and body size. *Mar. Ecol. Prog. Ser.* **506**, 99–113 (2014).

[32] Giering, S. L. C. *et al.* Seasonal variation of zooplankton community structure and trophic position in the Celtic Sea: A stable isotope and biovolume spectrum approach. *Prog Oceanogr* (2018).

[33] Thiebaux, M. L. & Dickie, L. M. Models of aquatic biomass size spectra and the common structure of their solutions. *J. Theor. Biol.* **159**, 147–161 (1992).

[34] Thiebaux, M. L. & Dickie, L. M. Structure of the body-size spectrum of the biomass in aquatic ecosystems: A consequence of allometry in predator-prey interactions. *Can. J. Fish.*

Aquat. Sci. **50**, 1308–1317 (1993).

[35] Sprules, W. G. & Munawar, M. Plankton size spectra in relation to ecosystem productivity, size, and perturbation. *Can. J. Fish. Aquat. Sci.* **43**, 1789–1794 (1986).

[36] Hutchinson, G. E. Homage to Santa Rosalia or why are there so many kinds of animals? *Am. Nat.* **93**, 145–159 (1959).

[37] Scheffer, M. & van Nes, E. H. Self-organized similarity, the evolutionary emergence of groups of similar species. *PNAS* **103**, 6230–6235 (2006).

[38] Rossberg, A. G., Rogers, T. & McKane, A. J. Are there species smaller than 1mm? *Proc. R. Soc. B* **280**, 20131248 (2013).

[39] Barabás, G., D'Andrea, R., Rael, R., Meszéna, G. & Ostling, A. Emergent neutrality or hidden niches? *Oikos* **122**, 1565–1572 (2013).

[40] Sakavara, A., Tsirtsis, G., Roelke, D. L., Mancy, R. & Spatharis, S. Lumpy species coexistence arises robustly in fluctuating resource environments. *PNAS* 201705944 (2017).

[41] D'Andrea, R. & Ostling, A. Challenges in linking trait patterns to niche differentiation. *Oikos* **125**, 1369–1385 (2016).

[42] Scheffer, M., van Nes, E. H. & Vergnon, R. Toward a unifying theory of biodiversity. *PNAS* **115**, 639–641 (2018).

[43] D'Andrea, R., Ostling, A. & O'Dwyer, J. P. Translucent windows: How uncertainty in competitive interactions impacts detection of community pattern. *Ecol Lett* **21**, 826–835 (2018).

[44] Cross, M. C. & Hohenberg, P. C. Pattern formation outside of equilibrium. *Rev Mod Phys* **65**, 851 (1993).

[45] Banas, N. S. Adding complex trophic interactions to a size-spectral plankton model: Emergent diversity patterns and limits on predictability. *Ecol. Model.* **222**, 2663–2675 (2011).

[46] Graner, F. & Dubrulle, B. Titius-Bode laws in the solar system. 1: Scale invariance explains everything. *Astron. Astrophys.* **282**, 262–268 (1994).

[47] Silvert, W. & Platt, T. Dynamic energy-flow model of the particle size distribution in pelagic ecosystems. In Kerfoot, W. C. (ed.) *Evolution and Ecology of Zooplankton Communities*, 754–763 (University Press of New England, Hanover, New Hampshire and London, England, 1980).

[48] Scott, F., Blanchard, J. L. & Andersen, K. H. Mizer: An R package for multispecies, trait-based and community size spectrum ecological modelling. *Methods Ecol. Evol.* **5**, 1121–1125 (2014).

[49] Blanchard, J. L. *et al.* Evaluating targets and trade-offs among fisheries and conservation objectives using a multispecies size spectrum model. *J. Appl. Ecol.* **51**, 612–622 (2014).

[50] Hartvig, M., Andersen, K. H. & Beyer, J. E. Food web framework for size-structured populations. *J. Theor. Biol.* **272**, 113–122 (2011).

[51] Houle, J. E., Farnsworth, K. D., Rossberg, A. G. & Reid, D. G. Assessing the sensitivity and specificity of fish community indicators to management action. *Can. J. Fish. Aquat. Sci.* **69**, 1065–1079 (2012).

[52] Rossberg, A. G., Houle, J. E. & Hyder, K. Stock-recruitment relations controlled by feeding interactions alone. *Can. J. Fish. Aquat. Sci.* **70**, 1447–1455 (2013).

[53] Andersen, K. H. & Beyer, J. E. Asymptotic size determines species abundance in the marine size spectrum. *Am. Nat.* **168**, 54–61 (2006).

[54] Hartvig, M. & Andersen, K. H. Coexistence of structured populations with size-based prey selection. *Theor Popul Biol* **89**, 24–33 (2013).

[55] Naisbit, R. E., Rohr, R. P., Rossberg, A. G., Kehrli, P. & Bersier, L.-F. Phylogeny versus body size as determinants of food-web structure. *Proc. R. Soc. B* **279**, 3291–3297 (2012).

[56] Nagelkerke, L. A. J. & Rossberg, A. G. Trophic niche-space imaging, using resource and consumer traits. *Theor. Ecol.* **7**, 423–434 (2014).

[57] Rossberg, A. G., Brännström, A. & Dieckmann, U. How trophic interaction strength depends on traits — A conceptual framework for representing multidimensional trophic niche spaces. *Theor. Ecol.* **3**, 13–24 (2010).

[58] Rossberg, A. G., Ishii, R., Amemiya, T. & Itoh, K. The top-down mechanism for body-mass–abundance scaling. *Ecology* **89**, 567–580 (2008).

[59] Zhang, L., Hartvig, M., Knudsen, K. & Andersen, K. H. Size-based predictions of food web patterns. *Theor Ecol* **7**, 23–33 (2013).

[60] Gaedke, U. The size distribution of plankton biomass in a large lake and its seasonal variability. *Limnol. Oceanogr.* **37**, 1202–1220 (1992).

[61] Gaedke, U. Identifying ecosystem properties: A case study using plankton biomass size distributions. *Ecol. Model.* **63**, 277–298 (1992).

[62] Shephard, S. *et al.* Size-selective fishing drives species composition in the Celtic Sea. *ICES J. Mar. Sci.* **69**, 223–234 (2012).

[63] Rossberg, A. G. & Farnsworth, K. D. Simplification of structured population dynamics in complex ecological communities. *Theor. Ecol.* **4**, 449–465 (2011).

[64] Cross, M. C. Structure of nonlinear traveling-wave states in finite geometries. *Phys. Rev. A* **38**, 3593–3600 (1988).

[65] Boudreau, P. R. & Dickie, L. M. Biomass spectra of aquatic ecosystems in relation to fisheries yield. *Can. J. Fish. Aquat. Sci.* **49**, 1528–1538 (1992).

[66] Tittel, J., Zippel, B., Geller, W. & Seeger, J. Relationships between plankton community structure and plankton size distribution in lakes of northern Germany. *Limnol. Oceanogr.* **43**, 1119–1132 (1998).

[67] Havlicek, T. & Carpenter, S. R. Pelagic species size distributions in lakes: Are they discontinuous? *Limnol. Oceanogr.* **46**, 1021–1033 (2001).

[68] Grimm, V. *et al.* Pattern-oriented modelling in population ecology. *Science of The Total Environment* **183**, 151–166 (1996).

[69] Newell, A. C., Passot, T. & Lega, J. Order parameter equations for patterns. *Annu Rev Fluid Mech* **25**, 399–453 (1993).

[70] Kirby, R. R. & Beaugrand, G. Trophic amplification of climate warming. *Proc. R. Soc. Lond. B Biol. Sci.* **276**, 4095–4103 (2009).

[71] Chust, G. *et al.* Biomass changes and trophic amplification of plankton in a warmer ocean. *Glob Change Biol* **20**, 2124–2139 (2014).

[72] Karban, R. Increased reproductive success at high densities and predator satiation for periodical cicadas. *Ecology* **63**, 321–328 (1982).

[73] Gaedke, U. & Straile, D. Daphnids: Keystone species for the pelagic food web structure and energy flow. - A body size-related analysis linking seasonal changes at the population and ecosystem levels. *Adv Limnol* **53**, 587–610 (1998).

[74] Cózar, A., García, C. M. & Gálvez, J. A. Analysis of plankton size spectra irregularities in two subtropical shallow lakes (Esteros del Iberá, Argentina). *Can. J. Fish. Aquat. Sci.* **60**, 411–420 (2003).

[75] Mantzavinos, C. Scientific explanation. SSRN Scholarly Paper ID 2782755, Social Science Research Network, Rochester, NY (2015).

[76] Hubbell, S. P. *The Unified Neutral Theory of Biodiversity and Biogeography* (Princeton University Press, Princeton, NJ, 2001).

[77] Strigul, N., Pristinski, D., Purves, D., Dushoff, J. & Pacala, S. Scaling from Trees to Forests: Tractable Macroscopic Equations for Forest Dynamics. *Ecol. Monogr.* **78**, 523–545 (2008).

[78] Purves, D. W., Lichstein, J. W., Strigul, N. & Pacala, S. W. Predicting and understanding forest dynamics using a simple tractable model. *PNAS* (2008).

[79] Shurin, J. B., Gruner, D. S. & Hillebrand, H. All wet or dried up? Real differences between aquatic and terrestrial food webs. *Proc. R. Soc. Lond. B Biol. Sci.* **273**, 1–9 (2006).

[80] Schwinghamer, P. Characteristic size distributions of integral benthic communities. *Can. J. Fish. Aquat. Sci.* **38**, 1255–1263 (1981).

[81] Duplisea, D. E. Benthic organism biomass size-spectra in the Baltic Sea in relation to the sediment environment. *Limnol Ocean.* **45**, 558–568 (2000).

[82] Holling, C. S. Cross-scale morphology, geometry, and dynamics of ecosystems. *Ecol. Monogr.* **62**, 447–502 (1992).

[83] Ho, J. C. & Michalak, A. M. Challenges in tracking harmful algal blooms: A synthesis of evidence from Lake Erie. *Journal of Great Lakes Research* **41**, 317–325 (2015).

[84] Tang, D., Kester, D. R., Ni, I.-H., Qi, Y. & Kawamura, H. In situ and satellite observations of a harmful algal bloom and water condition at the Pearl River estuary in late autumn 1998. *Harmful Algae* **2**, 89–99 (2003).

[85] Gaedke, U. & Kamjunke, N. Structural and functional properties of low- and high-diversity planktonic food webs. *J Plankton Res* **28**, 707–718 (2006).

[86] Edwards, K. F., Litchman, E. & Klausmeier, C. A. Functional traits explain phytoplankton community structure and seasonal dynamics in a marine ecosystem. *Ecol. Lett.* **16**, 56–63 (2013).

[87] Platt, T. & Denman, K. Organization in the pelagic ecosystem. *Helgoländer Wiss. Meeresunters.* **30**, 575–581 (1977).

[88] Platt, T. & Denman, K. The structure of pelagic ecosystems. *Rapp. P.-v. Réun. Cons. Int. Explor. Mer* **173**, 60–65 (1978).

[89] Blanco, J. M., Echevarria, F. & Garcia, C. M. Dealing with size-spectra: Some conceptual and mathematical problems. *Sci. Mar. Barc.* **58**, 17–29 (1994).

[90] Witek, Z. & Krajewska-Soltys, A. Some examples of the epipelagic plankton size structure in high latitude oceans. *J Plankton Res* **11**, 1143–1155 (1989).

[91] Echevarría, F. *et al.* The size-abundance distribution and taxonomic composition of plankton in an oligotrophic, high mountain lake (La Caldera, Sierra Nevada, Spain). *J Plankton Res* **12**, 415–422 (1990).

[92] Phillips, G. *et al.* Chlorophyll–nutrient relationships of different lake types using a large European dataset. *Aquat Ecol* **42**, 213–226 (2008).

[93] Kanda, J., Saino, T. & Hattori, A. Nitrogen uptake by natural populations of phytoplankton and primary production in the Pacific Ocean: Regional variability of uptake capacity. *Limnol. Oceanogr.* **30**, 987–999 (1985).

[94] Quinones, R. A., Platt, T. & Rodríguez, J. Patterns of biomass-size spectra from oligotrophic waters of the Northwest Atlantic. *Progress in Oceanography* **57**, 405–427 (2003).

[95] Chapra, S. C. & Dolan, D. M. Great Lakes total phosphorus revisited: 2. Mass balance modeling. *J. Great Lakes Res.* **38**, 741–754 (2012).

[96] Sprules, W. G. *et al.* Biomass size spectrum of the Lake Michigan pelagic food web. *Can. J. Fish. Aquat. Sci.* **48**, 105–115 (1991).

[97] Johengen, T. H., Johannsson, O. E., Pernie, G. L. & Millard, E. S. Temporal and seasonal trends in nutrient dynamics and biomass measures in Lakes Michigan and Ontario in response to phosphorus control. *Can. J. Fish. Aquat. Sci.* **51**, 2570–2578 (1994).

[98] de Eyto, E. & Irvine, K. Assessing the status of shallow lakes using an additive model of biomass size spectra. *Aquatic Conserv: Mar. Freshw. Ecosyst.* **17**, 724–736 (2007).

[99] Guildford, S. J., Bootsma, H. A., Taylor, W. D. & Hecky, R. E. High variability of phytoplankton photosynthesis in response to environmental forcing in oligotrophic lake Malawi/Nyasa. *J Great Lakes Res* **33**, 170–185 (2007).

[100] IGKB-Internationale Gewässerschutzkommission für den Bodensee. Zentrale Messdatenbank vom Bodensee - IGKB - Internationale Gewässerschutzkommission. https://www.igkb.org/aktuelles/bowis-bodensee-wasser-informations-system/zentrale-messdatenbank-vom-bodensee/ (2017).

[101] García, C. M., Echevarría, F. & Niell, F. X. Size structure of plankton in a temporary, saline inland lake. *J Plankton Res* **17**, 1803–1817 (1995).

[102] García, C. M. & Niell, F. X. Seasonal change in a saline temporary lake (Fuente de Piedra, southern Spain). *Hydrobiologia* **267**, 211–223 (1993).

[103] R Core Team. *R: A Language and Environment for Statistical Computing* (R Foundation for Statistical Computing, Vienna, Austria, 2017).

[104] Koenker, R. & Park, B. J. An interior point algorithm for nonlinear quantile regression. *J Econom* **71**, 265–283 (1996).

Acknowledgements. We thank Elvira de Eyto and Peder M. Yurista for making numerical size-spectrum datasets available for this study, and Stephen R. Carpenter, W. Gary Sprules, Jonathan B. Shurin, and Mark Trimmer for comments on earlier drafts of this paper. AGR was funded by the Natural Environment Research Council and the UK Department for Food, Environment and Rural Affairs (Defra) within the Marine Ecosystems Research Program (MERP, NE/L00299X/1).

Author contributions. AGR developed the non-linear SSSM and performed its mathematical analysis. AGR, UG and PK collected and critically evaluated literature data, and developed methods for model-data comparison. UG contributed unpublished data sets. All authors jointly wrote and edited the manuscript.

Competing interests. The authors declare no competing interests.

Materials & Correspondence. Axel G. Rossberg `<axel@rossberg.net>`

Supplementary Information

for

Dome patterns in pelagic size spectra reveal strong trophic cascades

Axel G. Rossberg, Ursula Gaedke, and Pavel Kratina

August 21, 2019

Contents

Supplementary Note 1: Definition of the non-linear Species Size-Spectrum Model

The non-linear SSSM builds on and generalises the linear SSSM that we presented in an earlier study [1]; below we refer to this study as 'CAT', base on the first few words on the paper's title ("A complete analytic theory..."), and provide pointers to relevant passages and equations for easy reference. In the present context, a 'linear' model means one where deviations of the size spectrum from an ideal power law are assumed to be so small that a linear approximation for the dynamics of these deviations is valid. By contrast, the non-linear SSSM admits arbitrary deviations of the size spectrum from an ideal power law. Its derivation follows that of the linear SSSM up to the point where the linearization is mathematically carried out. This derivation (extending over 24 pages) does not need to be repeated here. It leads to Equation [59] of CAT, an approximate formula for the momentary linear growth rate $\Lambda(m_*)$ of populations of species with maturation body mass m_* (there written as "$\langle V_{m_*}|L_{m_*}W_{m_*}\rangle$"):

$$\Lambda(m_*) = \int_0^\infty \left[(\alpha f(m)h - k)m^n - m\,\mu_p(m)\right] W_{m_*}(m)dm. \tag{1}$$

In this integral, m denotes the body mass of individuals (independent of their species identity); $f(m)$ denotes their feeding level (a number between 0 and 1 quantifying the degree of satiation); α is the assimilation efficiency; h and k are coefficients scaling maximum intake rate and respiration rate, respectively; the factor m^n describes the allometric scaling of these rates with body mass; $\mu_p(m)$ is the predation mortality at body size m; and $W_{m_*}(m)$ represents the size structure of populations with maturation body size m_*, normalised to unit population biomass ($\int mW_{m_*}(m)dm = 1$). Parameter values and formulae for computing the functions $f(m)$, $\mu_p(m)$, and $W_{m_*}(m)$ are given in Supplementary Table 1. The computation consists of several steps, which are illustrated in Supplementary Figure 1.

The derivation of Eq. (1) makes use of an approximation that, except for variations in maturation body size m_*, all individuals of a given size m are ecologically equivalent. Further, it takes into account (i) that an accurate unstructured model for the dynamics of a structured populations can be obtained by tracking gains and losses in the total reproductive value [4] of that population [5, 3], and (ii) that in simple size-structured models, such as the one underlying Eq. (1), the reproductive value of individuals is proportional to their body mass [6, Section 6.4.3] and so total reproductive value proportional to population biomass. Hence, the term in brackets in Eq. (1) evaluates biomass gains (somatic growth and reproduction) and losses (mortality) by individuals of size m. These are then summed up for populations of species with a given maturation body size m_* and corresponding population structure $W_{m_*}(m)$.

The non-linear SSSM describes the dynamics of the density $B(m_*)$ of community biomass along the linear m_*-axis. That is, for any maturation body mass interval $[m_*, m_* + \Delta m_*]$ that is not too wide (e.g. $\Delta m_* \ll m_*$), the total biomass (or spatial biomass density) of all species in

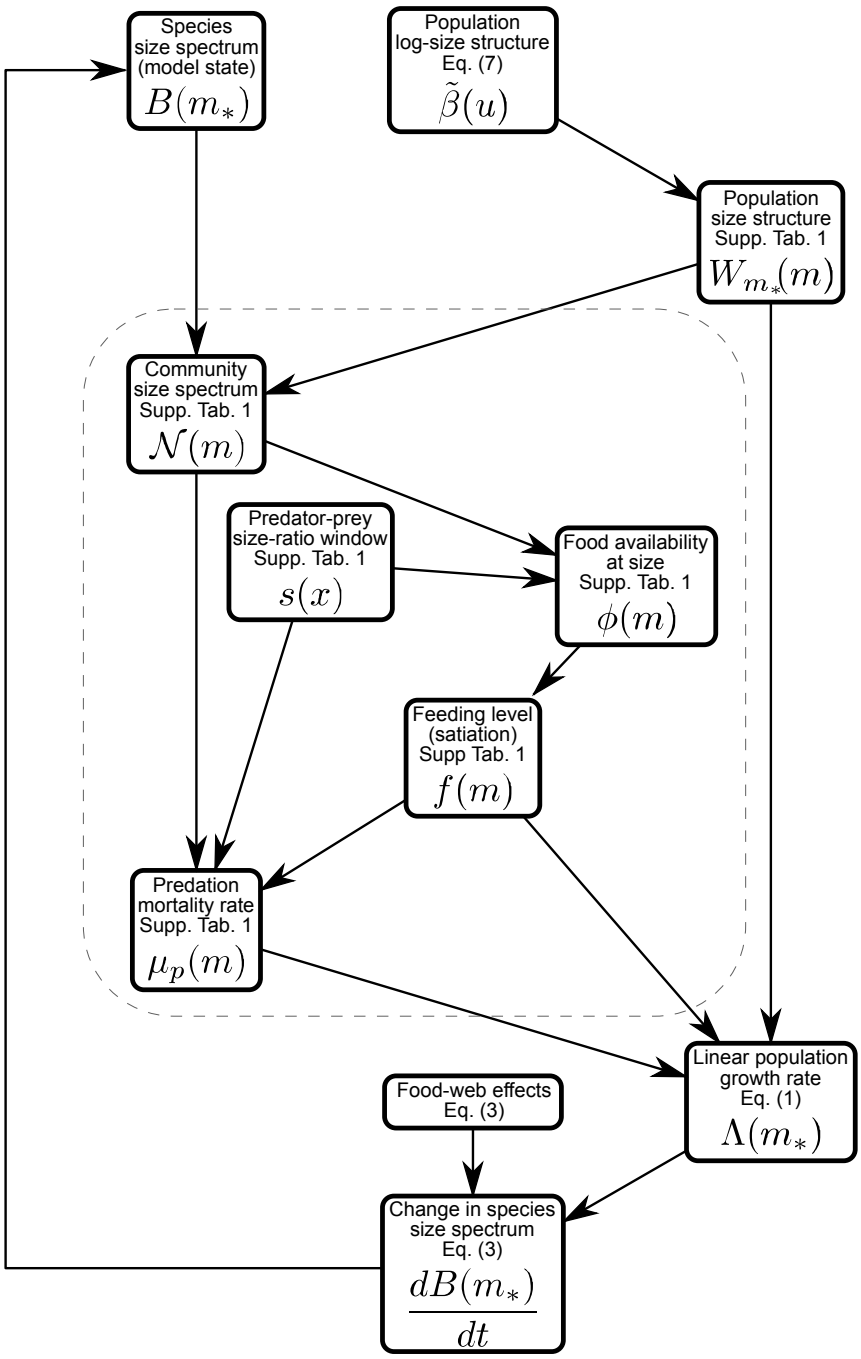

Supplementary Figure 1: Dependencies between size-dependent quantities in the definition of the SSSM. Arrows indicate how each quantity enters the formula for other quantities. The dependencies enclosed by the dashed line follow the model of Ref. [2]. The other dependencies follow from the application of the quasi-neutral approximation [3] to this model, derived in CAT.

a community that have maturation body mass in this interval is $B(m_*)\Delta m_*$. From $B(m_*)$, one can compute the density of biomass along the $(\ln m_*)$-axis as $m_* B(m_*)$, the density of individuals along the linear m-axis $\mathcal{N}(m)$ (Supplementary Table 1), the density of biomass along the linear body mass axis (the so-called normalised *community size spectrum*) as $m\mathcal{N}(m)$, and the density of biomass along the $(\ln m)$-axis, computed as $m^2\mathcal{N}(m)$, which is the representation used in the main text.

In principle, dynamics in the model are given by the simple equation

$$\frac{dB(m_*)}{dt} = \Lambda(m_*)B(m_*). \tag{2}$$

However, in order to suppress artefacts resulting from modelling a food-web with distinct species by a continuum of species characterised by size alone, CAT (Section 6.4) adds a term that damps fluctuations on small scales along the $(\ln m_*)$-axis, resulting in the modified dynamic equation

$$\begin{aligned}\frac{dB(m_*)}{dt} =& \Lambda(m_*)B(m_*)+ \\ & \rho m_*^{n-1}\left\{ B(m_*)\exp\left[\frac{\sigma_r^2(\lambda-2)^2}{2}\right] - \frac{\displaystyle\int_0^\infty B(m'_*)\exp\left[-\frac{\log^2\left(\frac{m'_*}{m_*}\right)}{2\sigma_r^2}\right]dm'_*}{m_*\sqrt{2\pi}\sigma_r}\right\}\end{aligned} \tag{3}$$

(see Supplementary Table 1 for the values of λ, σ_r and ρ). The added correction appears complex here because we write it for a linear m_* scale. When going over to logarithmic size variables, it simplifies considerably, see Eq. (26) below. The role of the additional term is to suppress a model artefact that arises from model simplifications (called coarse graining in the literature) that amount to the assumption that the strength of feeding interactions depends only on the body sizes of consumers and resources. When this dependence is continuous in both resource and consumer body sizes (as it is here), this assumption implies that species of very similar size have very similar consumers and resources and therefore compete strongly with each other. This strong competition among species of similar sizes means that the biomass in a narrow species size class can arbitrarily grow (or decline) while the biomass of a narrow neighbouring species size class declines (or grows), without otherwise affecting community dynamics, as long as the total biomass in the two species size classes remains constant. Minute irregular deviations from this neutral competition will lead to irregular increases and decreases of biomasses of species of similar size, resulting in a ragged species size spectrum that is smooth

only when averaged over sufficiently wide intervals on the log-species-size axis. In reality food webs are more complex because traits other than body mass matter as well [7]. Two species of similar size can therefore have very different sets of consumers and resources, and then do not directly compete with each other. Frequent competitive exclusion of species of similar size would only occur for (hypothetical) communities that are excessively over-saturated with species. Competitive exclusion would then lead to extinction of species until a (near) natural species richness is reached. Natural communities are in such a state: whenever competitive exclusion would happen, it has (mostly) happened already. In natural communities competition between species of similar size is therefore smaller than expected from the simplifying assumption that body-size alone controls feeding interactions.

The correction term puts this right by damping modulations of small wavelength along the species size spectrum. It is constructed such that dynamics on scales much longer than σ_r along the $(\ln m_*)$-axis are not affected. The parameter ρ controls the strength of the suppression of artificial competitive exclusion amongst species of similar size in the model. The particular form of the correction and constraints on the parameters were derived in CAT based on heuristic ecological considerations. A systematic analytical derivation of the correction from first principles would require a better understanding of food-web structure and dynamic than we currently have.

The transition from the linear to the non-linear SSSM permits introduction of a boundary condition representing the upper cutoff of the species size spectrum, above which abundances decline to zero. This is done by simply fixing

$$B(m_*) = 0 \qquad \text{for } m_* > m_{*\max}, \tag{4}$$

with $m_{*\max}$ representing the maturation body mass of the largest species present in the community.

The lower boundary condition is implemented in the model by fixing

$$B(m_*) = x\tilde{B}_{\text{tot}} m_*^{1-\lambda} \qquad \text{for } m_* < m_{*\min}. \tag{5}$$

The constant $\tilde{B}_{\text{tot}}$ is chosen such that $B(m_*) = \tilde{B}_{\text{tot}} m_*^{1-\lambda}$ corresponds to the ideal equilibrium power-law species size spectrum in the so called *oligotrophic regime* of the model, where the feeding level $f(m) = f_0$ is the same for all body sizes m, with some constant $0 < f_0 < 1$ (CAT, Section 2.1 and p. 457). It is given by

$$\tilde{B}_{\text{tot}} = \frac{\tilde{\mathcal{N}}}{\int_{-\infty}^{\infty} \mathrm{e}^{(\lambda-2)u} \tilde{\beta}(u) du}, \tag{6a}$$

where

$$\tilde{\mathcal{N}} = \frac{k}{\sqrt{2\pi}\gamma\sigma_s \left\{ \beta^{n-1} \mathrm{e}^{(n-1)^2\sigma_s^2/2} - \left(\alpha - \frac{k}{h}\right) \beta^{\lambda-2} \mathrm{e}^{(\lambda-2)^2\sigma_s^2/2} \right\}} \tag{6b}$$

is the corresponding power-law coefficient for the community size spectrum. The dimensionless scale factor x in Eq. (5) can be varied to represent variations in trophic state. To achieve a smooth transition between m_*-ranges of fixed $B(m_*)$ for $m_* < m_{*\mathrm{min}}$ and dynamic $B(m_*)$ for $m_{*\mathrm{min}} \leq m_* \leq m_{*\mathrm{max}}$, a further damping term $-0.5\mathrm{g}^{1-n}\mathrm{yr}^{-1}\, m_*^{n-1}[B(m_*) - y\tilde{B}_{\mathrm{tot}} m_*^{1-\lambda}]/[1 + (m_*\beta^{-1}m_{*\mathrm{min}}^{-1})^{1/2}]$ is added on the right-hand side of Eq. (3), following CAT (Section 8.2). It affects dynamics only for $m_* \lesssim \beta m_{*\mathrm{min}}$, with β representing the typical predator-prey mass ratio.

Supplementary Note 2: Model parameterization

Because of several simplifications of empirical laws invoked in the construction of the SSSM, one cannot expect there to be a "correct" set of values for the model's life-history and physiological parameters that could be determined through direct measurements. Instead, the question we ask here when discussing the model's parameterization is just whether the values we did choose are broadly in line with the numerical ranges observed for corresponding empirical parameters. Our choices of model parameters (Supplementary Table 1) are based on those by [2] and CAT (Section 8.1), with some modifications required to make the model more representative of pelagic communities and to reproduce the empirical characteristics of dome formation. When there was a choice, we preferred values representative of zooplankton, as zooplankters are intermediate within the range of characteristics relevant for pelagic size spectra.

Compared to [2], the allometric coefficient for metabolic losses was reduced by a factor 4 to $2.5\mathrm{g}^{1-n}\mathrm{yr}^{-1}$. The empirical value for this parameter depends on body architecture [8]. Our choice comes closer to that found for copepods, while the original value was rather representative of fish [8, Fig. 1b]. The parameter specifying the preferred predator-prey mass ratio was raised to $\beta = 500$ from 100. Both values are compatible with the empirical range of values for aquatic organisms in general [9, Fig. 3] and for planktonic predators in particular [10, Fig. 3]. In line with the increase in β, the width of the predator-prey mass ratio window on the $\ln(m)$ scale was increased to $\sigma_s = 1.5$ from 1. Assimilation efficiency was reduced from 0.6 to $\alpha = 0.3$, a typical value for zooplankton [11, Tab. 1]. The allometric exponent for search&attack rates was increased from $p = 0.8$ to $p = 0.9$ to better reproduce observed values around -1.10 for the slope $-1-p+n$ of normalised size spectra at low nutrient levels [12, 13]. The coefficient γ for search&attack rates was adjusted from $1.6 \times 10^4\,\mathrm{g}^{1-q}\mathrm{m}^{-3}\mathrm{yr}^{-1}$ [2, Eq. 16] to $10^5\,\mathrm{g}^{1-q}\mathrm{m}^{-3}\mathrm{yr}^{-1}$ to account for our quantification of biomass in terms of carbon rather than wet weight and to

reproduce observed biomass density in pelagic systems (Fig. 3a). The value of the coefficient of the damping term in Eq. (3) is constrained only by a dimensional analysis. It has the same dimensions as the coefficients of the rates of food-intake h and metabolic losses r. Combining these, one obtains a corresponding coefficient for the maximum rate of food assimilation minus losses, $\alpha h - r$. In our parameterization, this evaluates to $23\,\mathrm{g}^{1-n}\mathrm{yr}^{-1}$. Our choice $\rho = 10\,\mathrm{g}^{1-n}\mathrm{yr}^{-1}$ is consistent with the expectation that ρ is of similar magnitude. The heuristic argument of CAT to constrain the width of the size range of damping, σ_r, suggests it should be of the magnitude of the typical distance on the $(\ln m_*)$-axis between the main predators or prey of a species. Assuming that a typical consumer has approximately three prey species making a major contribution the diet [14, 6] (and fewer "main" predators), and noting that we set the width of the predator-prey mass ratio window to $\sigma_s = 1.5$, our choice $\sigma_r = 0.5 = \sigma_s/3$ is consistent with these considerations.

Finally, the simple approximation derived in CAT (Eq. [114]) for the distribution $\tilde{\beta}(u)$ of a species' biomass over the logarithmic body size axis $u = \ln(m/m_*)$ was replaced by

$$\tilde{\beta}(u) = \frac{\eta(1-n)}{\eta + (1-n)\eta^n - \eta x_0^{1-n}} \begin{cases} 0 & \text{if } \exp(u) < x_0, \\ \mathrm{e}^{u(1-n)} & \text{if } x_0 \le \exp(u) < 1, \\ \dfrac{\mathrm{e}^{(2-n)u/(1-n)}\eta^n(\mathrm{e}^{-u}\eta^n - \mathrm{e}^{-nu}\eta)^{1/(1-n)}}{(\eta^n - \eta)^{1/(1-n)}[(\mathrm{e}^u\eta)^n - \mathrm{e}^u\eta]} & \text{if } 1 \le \exp(u) < \eta^{-1}, \\ 0 & \text{if } \eta^{-1} \le \exp(u). \end{cases} \tag{7}$$

This expression describes a steady-state size distribution of individuals that, after being born at size $x_0 m_*$, utilise all assimilated food for maintenance and growth until they reach maturation at size m_*, from where on they invest a proportion $(\eta m/m_*)^{1-n}$ of available energy into reproduction. Such a maturation schedule implies von Bertalanffy growth trajectories for $m > m_*$ [2]. Equation (7) above follows from a metabolic model according to formula (9) of [2] in the limit of infinitely fast maturation. In this limit, a complicated but explicit expression for the Fourier transformation of $\tilde{\beta}(u)$ can be computed using symbolic algebra software, which is an important step when studying the SSSM analytically. The graph of $\tilde{\beta}(u)$ is shown in Supplementary Figure 2. In this graph, the sudden increase of biomass density above $m = m_*$ reflects the sudden slowing down of growth after maturation (as on a congested highway). The subsequent decline of density results from the thinning of ever-slower growing cohorts by predation. The ratio of offspring to maturation body mass x_0 was set to 0.02, consistent with results for invertebrates of around $1\,\mu\mathrm{gC}$ from an independent meta-analysis [15, Fig. 3]

The dynamic maturation body-mass range is chosen as $m_{*\mathrm{min}} = 20\,\mathrm{pgC}$, $m_{*\mathrm{max}} = 10\,\mathrm{kgC}$, representing a typical size range from phytoplankton to large fish in lakes.

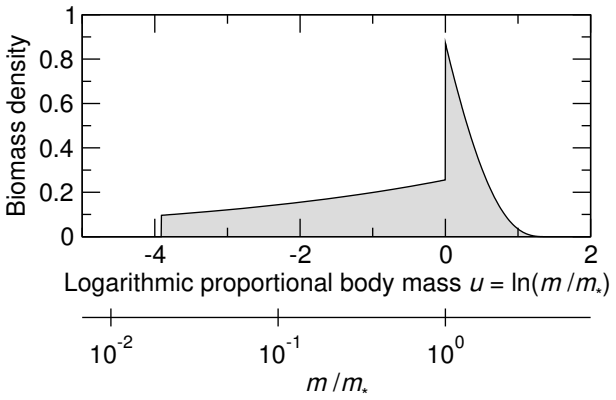

Supplementary Figure 2: Assumed distribution a population's biomass over the logarithmic body mass axis. The value $u = 0$ corresponds to the body mass at first maturation. The curve is given by Eq. (7) with $x_0 = 0.02$, $\eta = 1/4$ and $n = 3/4$.

Supplementary Table 1: Details of model definition and parameters. For an illustration of the dependencies between size-dependent quantities, see Supplementary Figure 1.

Symbol	Value	Interpretation
α	0.3	Assimilation efficiency
β	500	Preferred predator-prey mass ratio
$\tilde{\beta}(u)$	Eq. (7)	Biomass density of population on $u = \ln(m/m_*)$ axis, scaled to $\int \tilde{\beta}(u)du = 1$
γ	$10^5\,\mathrm{g}^{1-q}\mathrm{m}^{-3}\mathrm{yr}^{-1}$	Coefficient of search&attack rate
λ	$2 + q - n$	Size-spectrum exponent in oligotrophic regime
$\mu_p(m_p)$	$\int_0^\infty s\left(\ln\frac{m}{m_p}\right)[1 - f(m)]\gamma m^q \mathcal{N}(m)dm$	Predation mortality of species of size m_p
σ_r	0.5	Body size range for food-web effects
σ_s	1.5	Width of predator-prey size-ratio window
η	0.25	Maturation- over asymptotic body mass
$\phi(m)$	$\int_0^\infty m_p \mathcal{N}(m_p) s\left(\ln\frac{m}{m_p}\right) dm_p$	Food available to individuals of size m
$\tilde{B}_{\mathrm{tot}}$	Eq. (6a)	Coefficient of ideal oligotrophic power-law species size spectrum

(continued on next page)

Supplementary Table 1 (continued)

Symbol	Value	Interpretation
$f(m)$	$\dfrac{\gamma m^q \phi(m)}{\gamma m^q \phi(m) + h m^n}$	Feeding level of species of size m
h	$85\,\mathrm{g}^{1-n}\mathrm{yr}^{-1}$	Coefficient of maximal food intake
k	$2.5\,\mathrm{g}^{1-n}\mathrm{yr}^{-1}$	Coefficient of metabolic loss rate
$\mathcal{N}(m)$	$\int_0^\infty B(m_*) W_{m_*}(m) dm_*$	Community size spectrum
m	variable	Individual body mass
m_p	variable	Body mass of prey individual
m_*	variable	Maturation body mass
$m_{*\mathrm{min}}$	$20\,\mathrm{pg}$	Lower cutoff of species size spectrum
$m_{*\mathrm{max}}$	$10\,\mathrm{kg}$	Upper cutoff of species size spectrum
n	0.75	Allometric exponent of respiration
$\tilde{\mathcal{N}}$	Eq. (6b)	Coefficient of ideal oligotrophic power-law community size spectrum
q	0.9	Allometric exponent of search/attack rate
ρ	$10\,\mathrm{g}^{1-n}\mathrm{yr}^{-1}$	Strength of food-web effects
$s(x)$	$\exp\left[-(x - \ln\beta)^2/(2\sigma_s^2)\right]$	Predator-prey mass-ratio window
$W_{m_*}(m)$	$m^{-2}\tilde{\beta}(\ln(m/m_*))$	A population's density of individuals on m-axis, scaled to $\int m W_{m_*}(m) dm = 1$
x_0	0.02	Body mass of offspring relative to m_*

Supplementary Note 3: Model Simulations

For numerical simulations of size-spectrum dynamics, the $\log_{10}(m_*)$ and $\log_{10}(m)$-axes were discretized to $N = 512$ lattice points separated by 0.05 starting from $m_* = m_{*\mathrm{min}}$. Evaluation of $\Lambda(m_*)$, given by Eq. (1) and Supplementary Table 1, requires computation of several nested integrals over m_* and m in each simulation time step (Supplementary Figure 1). We approximated these integrals by midpoint Riemann sums over the simulation lattice, and made use of the simplifying allometric scaling assumptions for life-history traits in Supplementary Note 1 to convert these sums into discrete convolution operations, which were evaluated using fast Fourier transforms. This reduced the computational cost of the model from $\mathcal{O}(N^2)$ to $\mathcal{O}(N \log N)$ per simulation time step. The resulting system of ODEs was simulated using the solver CVODE from the SUNDIALS package [16], which automatically adjusted approximation order and step size to achieve our prescribed accuracy of 10^{-4} per step for $\ln B(m_*)$. In addition, upper limits

on step size, scaling as the square-root of time since the start of simulations, were imposed to avoid numerical instability (CAT, Sec. 8.2).

The initial condition for each simulation was taken to be x times the ideal oligotrophic power-law size spectrum $\tilde{B}_{\mathrm{tot}} m_*^{1-\lambda}$. Because for large x the size spectra can exhibit periodic or irregular dynamics, simulations were first run with a burn-in of 20 years, before 100 snapshots taken in 1-year intervals were evaluated to compute medians and quantile ranges of the characteristics, B_0, S, A, and D in Fig. 3.

Supplementary Note 4: Empirical size spectra and fitted modulated lines

In the following, we show the graphs of all 25 empirical size spectra included in this study (open circles), together with the linear-plus-sinusoidal fits (red lines) described in the main text. Since only data up to $0.1\mathrm{gC}$ body mass were used for the model fits (Materials Methods), the red lines are restricted to this range. For easy comparison, all graph have identical horizontal axes and identically scaled vertical axes. The spectra are shown in the order in which they were listed in Materials and Methods: approximately sorted by increasing nutrient concentration, while keeping related spectra together.

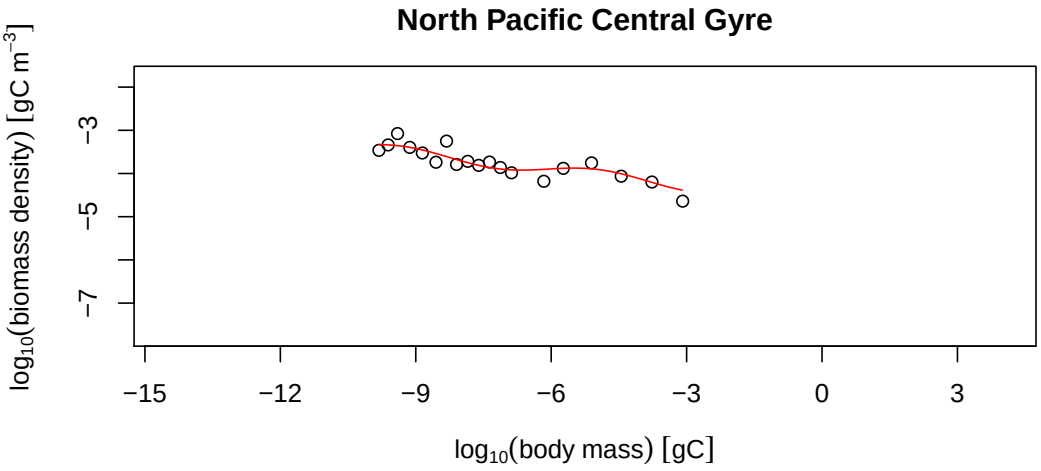

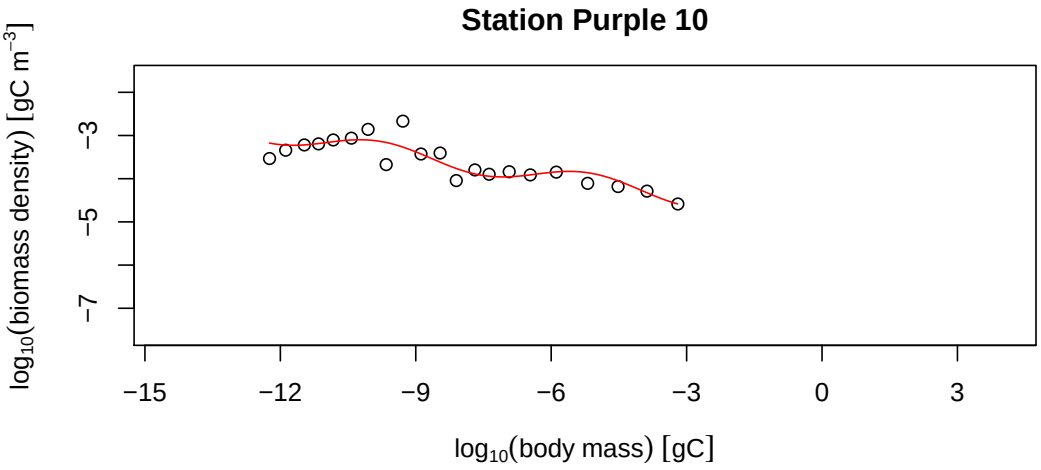
Station Purple 10
log10(biomass density) [gC m−3]
−3
−5
−7
−15
−12
−9
−6
−3
0
3
log10(body mass) [gC]

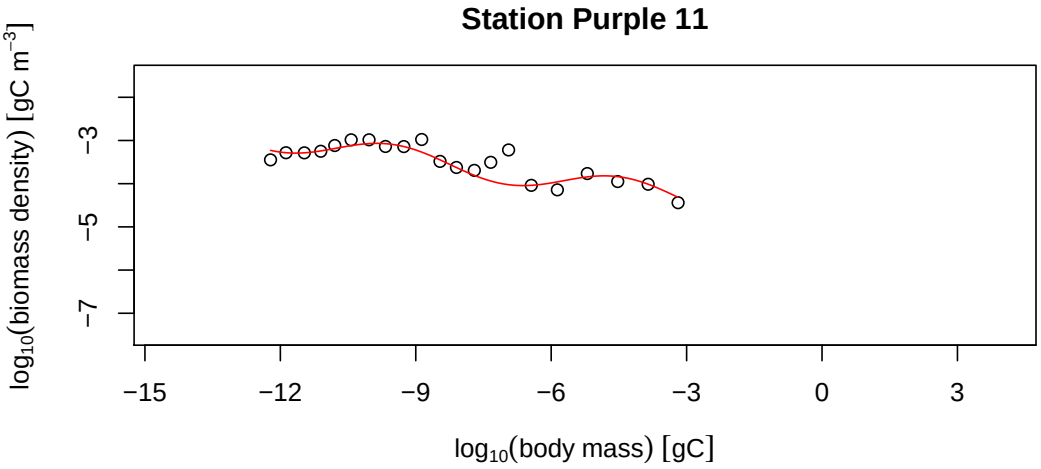
Station Purple 11
log10(biomass density) [gC m−3]
−3
−5
−7
−15
−12
−9
−6
−3
0
3
log10(body mass) [gC]

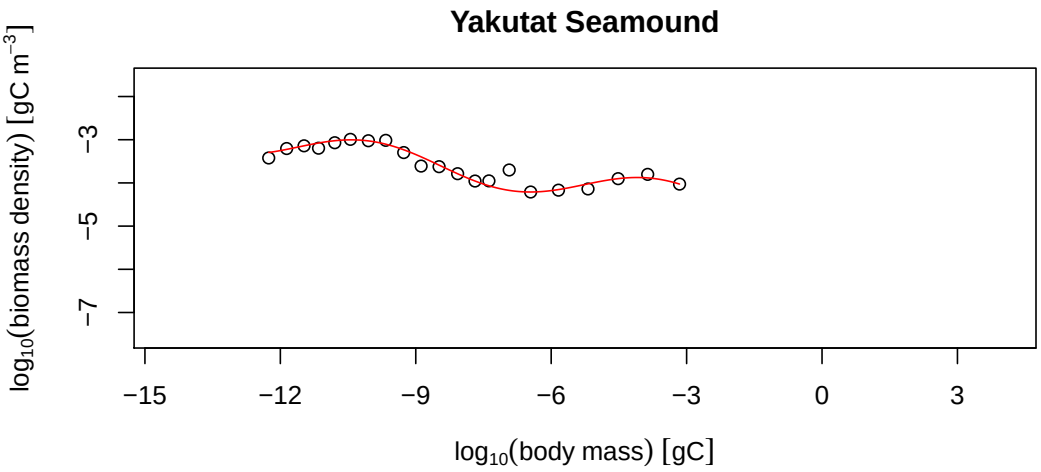
Yakutat Seamound
log10(biomass density) [gC m−3]
−3
−5
−7
−15
−12
−9
−6
−3
0
3
log10(body mass) [gC]

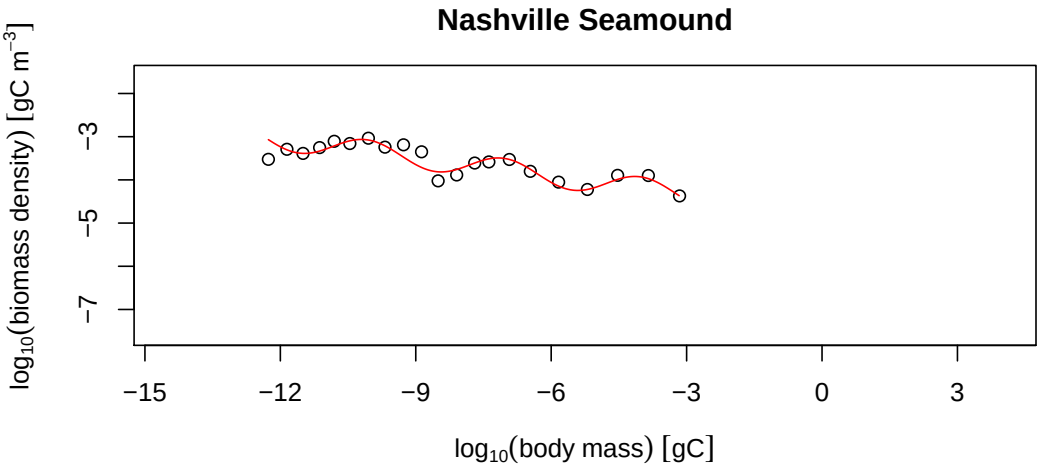
Nashville Seamound
log10(biomass density) [gC m−3]
−3
−5
−7
−15
−12
−9
−6
−3
0
3
log10(body mass) [gC]

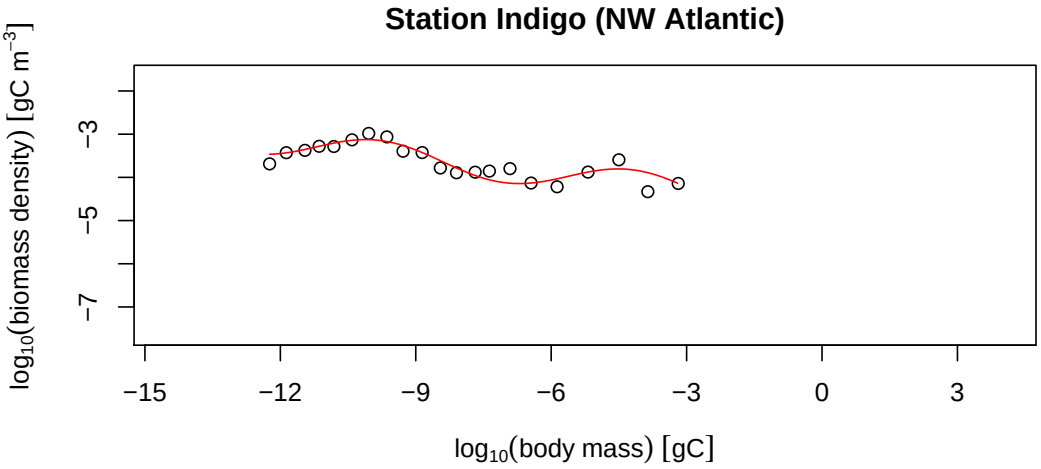
Station Indigo (NW Atlantic)
log10(biomass density) [gC m−3]
−3
−5
−7
−15
−12
−9
−6
−3
0
3
log10(body mass) [gC]

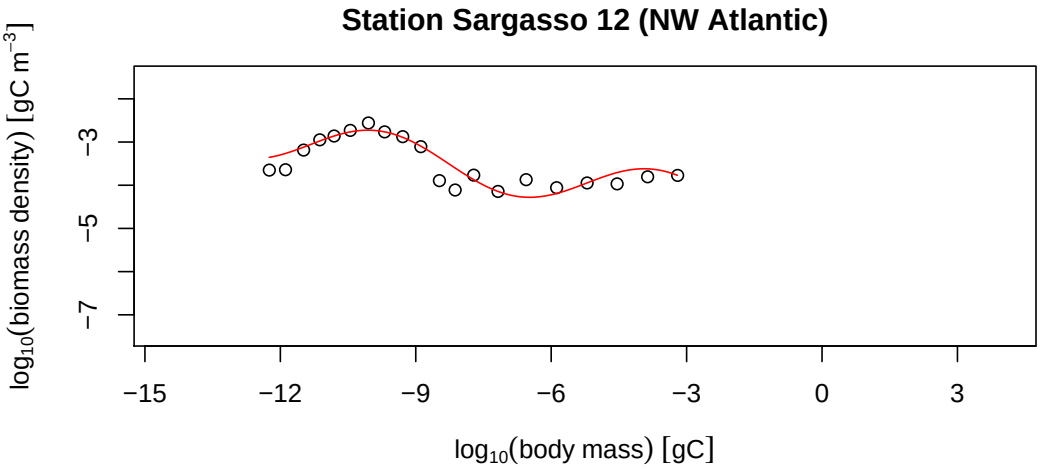
Station Sargasso 12 (NW Atlantic)
log10(biomass density) [gC m−3]
−3
−5
−7
−15
−12
−9
−6
−3
0
3
log10(body mass) [gC]

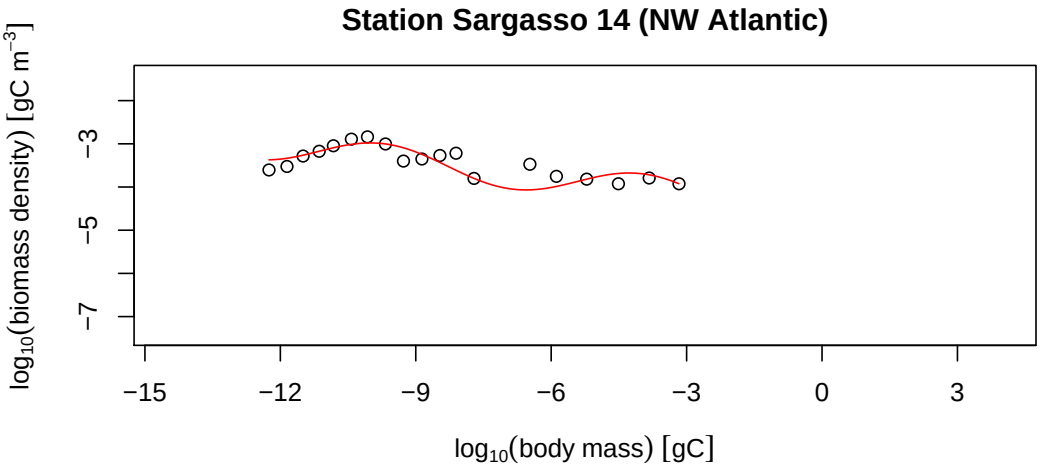
Station Sargasso 14 (NW Atlantic)
log10(biomass density) [gC m−3]
−3
−5
−7
−15
−12
−9
−6
−3
0
3
log10(body mass) [gC]

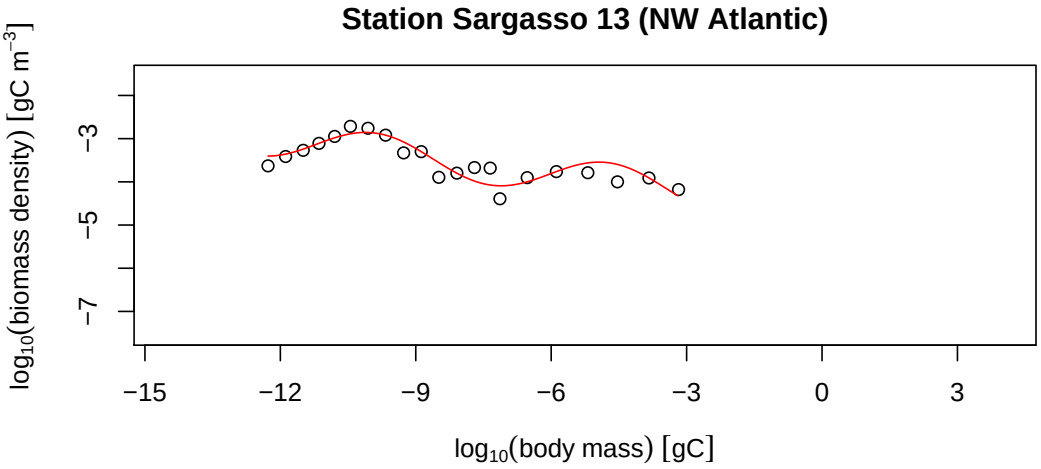
Station Sargasso 13 (NW Atlantic)
log10(biomass density) [gC m−3]
−3
−5
−7
−15
−12
−9
−6
−3
0
3
log10(body mass) [gC]

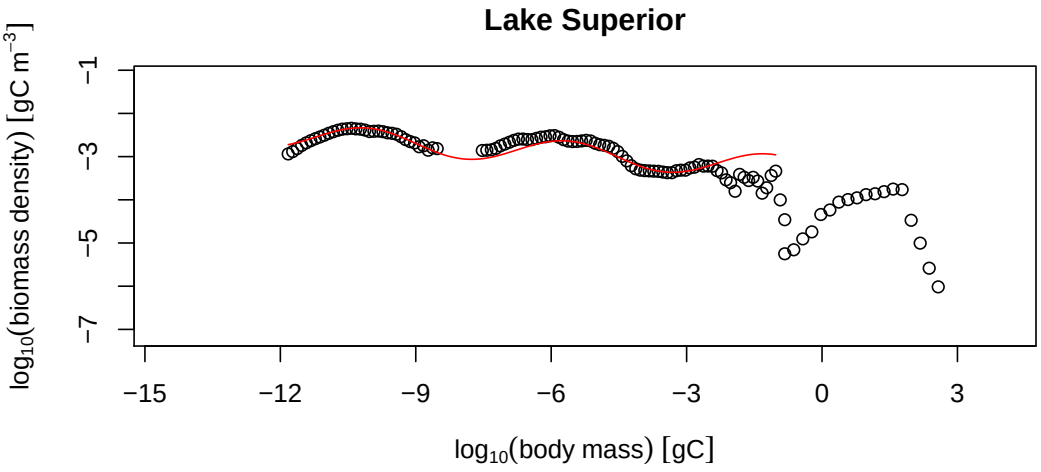
Lake Superior
log10(biomass density) [gC m−3]
−1
−3
−5
−7
−15
−12
−9
−6
−3
0
3
log10(body mass) [gC]

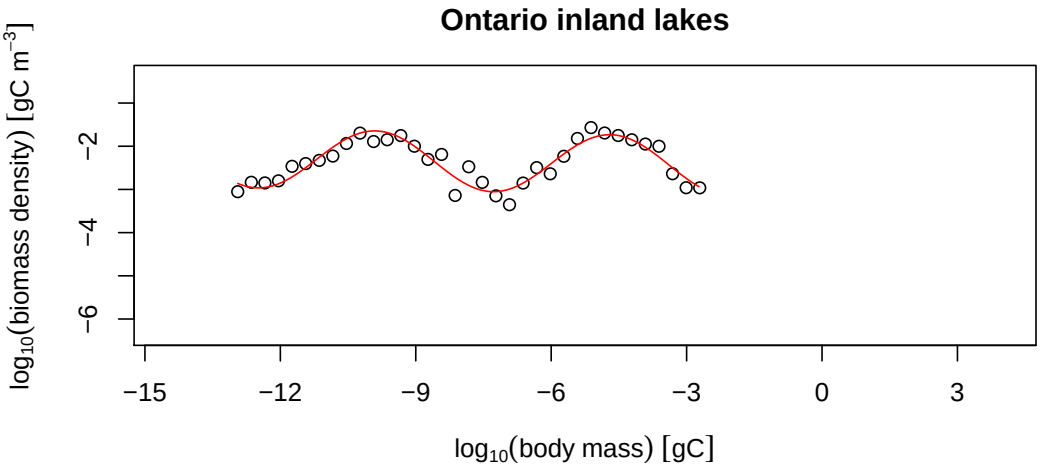
Ontario inland lakes
log10(biomass density) [gC m−3]
−2
−4
−6
−15
−12
−9
−6
−3
0
3
log10(body mass) [gC]

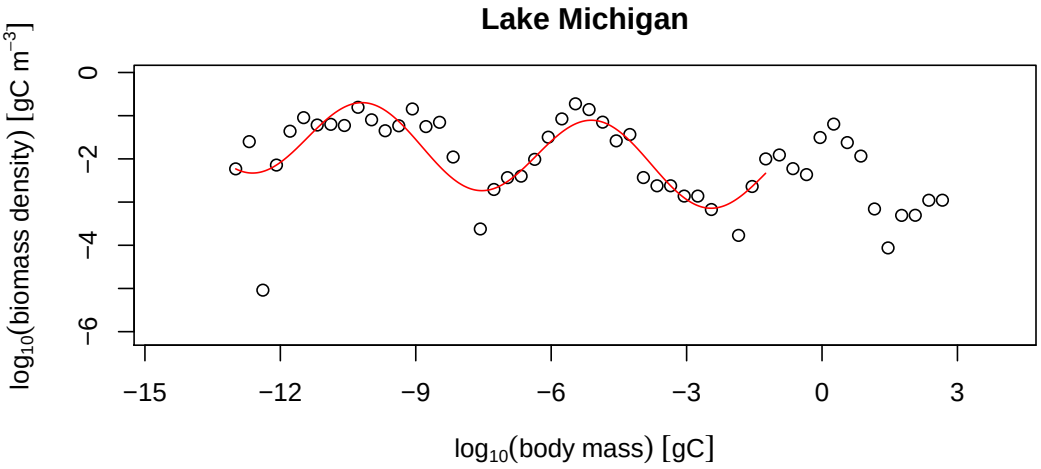
Lake Michigan
log10(biomass density) [gC m−3]
0
−2
−4
−6
−15
−12
−9
−6
−3
0
3
log10(body mass) [gC]

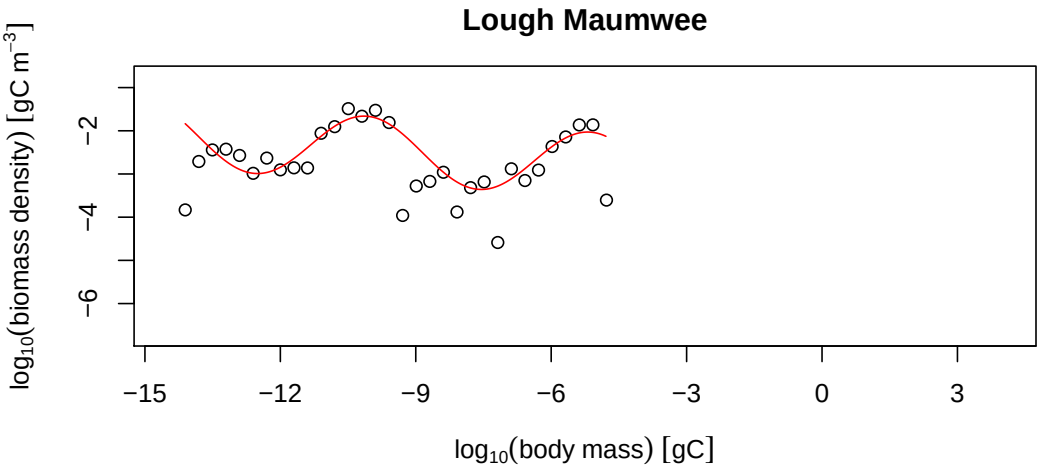
Lough Maumwee
log10(biomass density) [gC m−3]
−2
−4
−6
−15
−12
−9
−6
−3
0
3
log10(body mass) [gC]

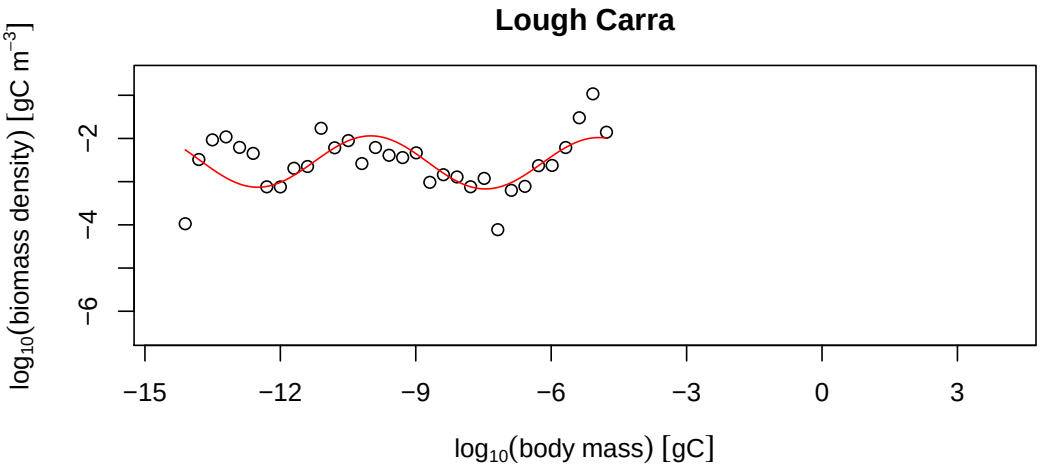
Lough Carra
log10(biomass density) [gC m−3]
−2
−4
−6
−15
−12
−9
−6
−3
0
3
log10(body mass) [gC]

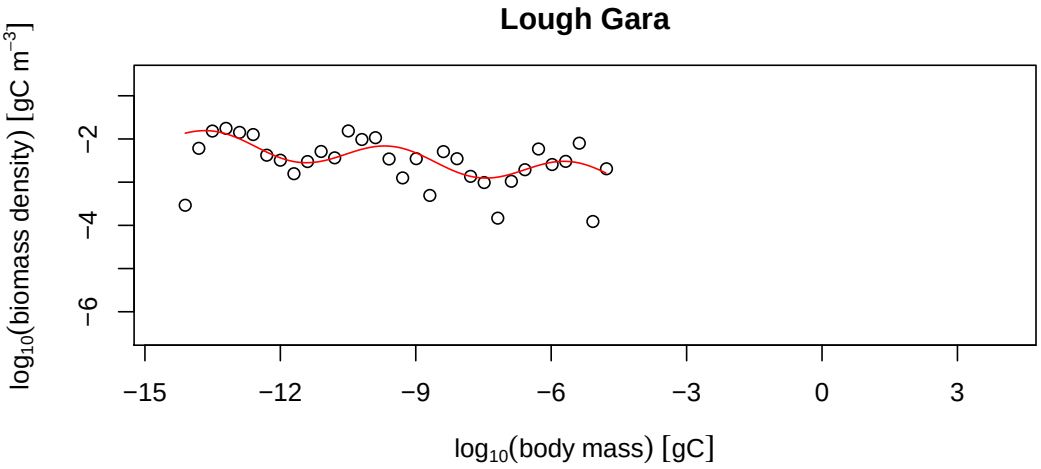
Lough Gara
log10(biomass density) [gC m−3]
−2
−4
−6
−15
−12
−9
−6
−3
0
3
log10(body mass) [gC]

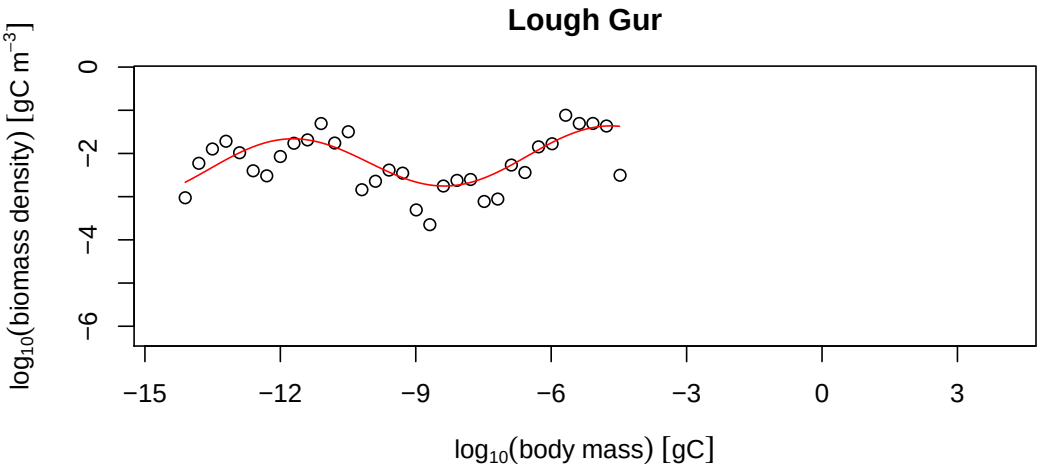
Lough Gur
log10(biomass density) [gC m−3]
0
−2
−4
−6
−15
−12
−9
−6
−3
0
3
log10(body mass) [gC]

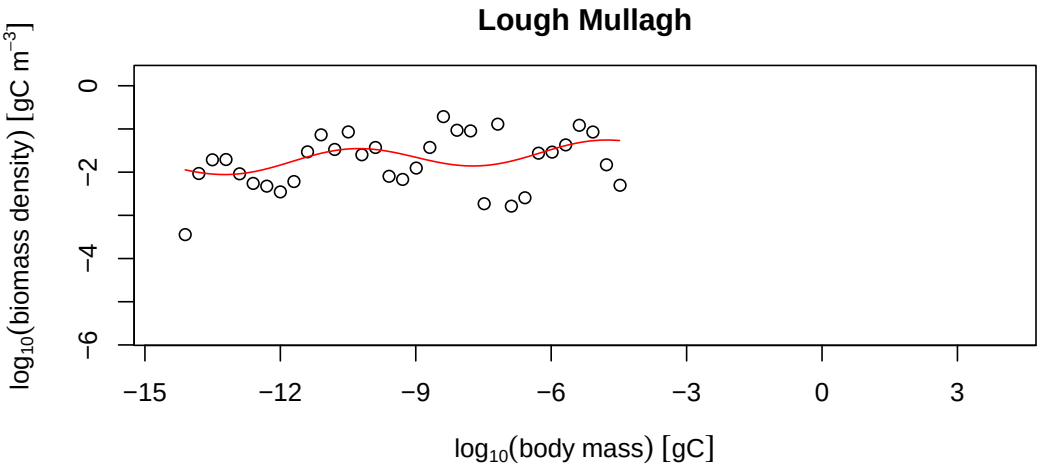
Lough Mullagh
log10(biomass density) [gC m−3]
0
−2
−4
−6
−15
−12
−9
−6
−3
0
3
log10(body mass) [gC]

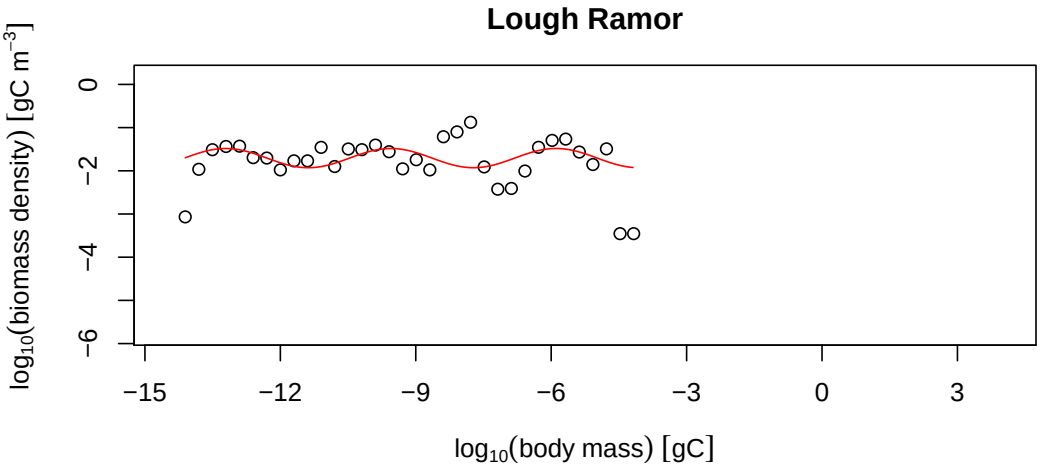
Lough Ramor
log10(biomass density) [gC m−3]
0
−2
−4
−6
−15
−12
−9
−6
−3
0
3
log10(body mass) [gC]

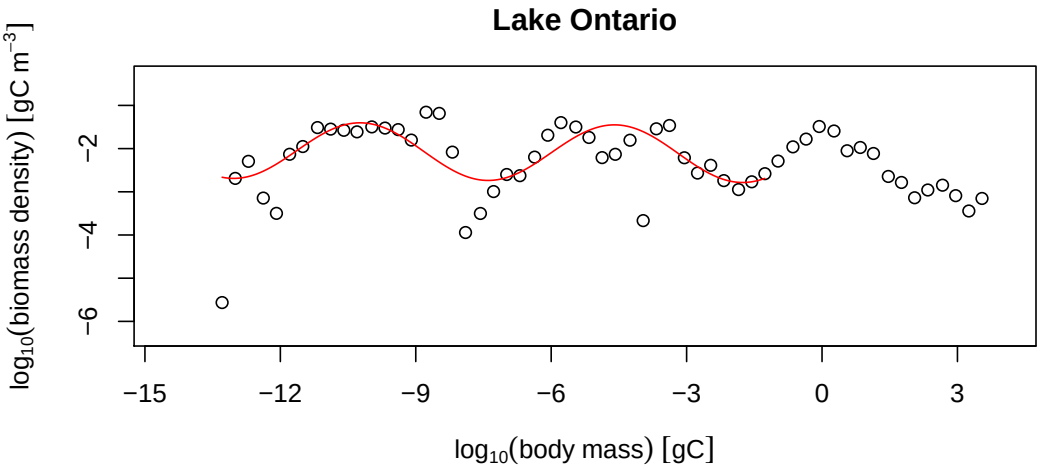
Lake Ontario
log10(biomass density) [gC m−3]
−2
−4
−6
−15
−12
−9
−6
−3
0
3
log10(body mass) [gC]

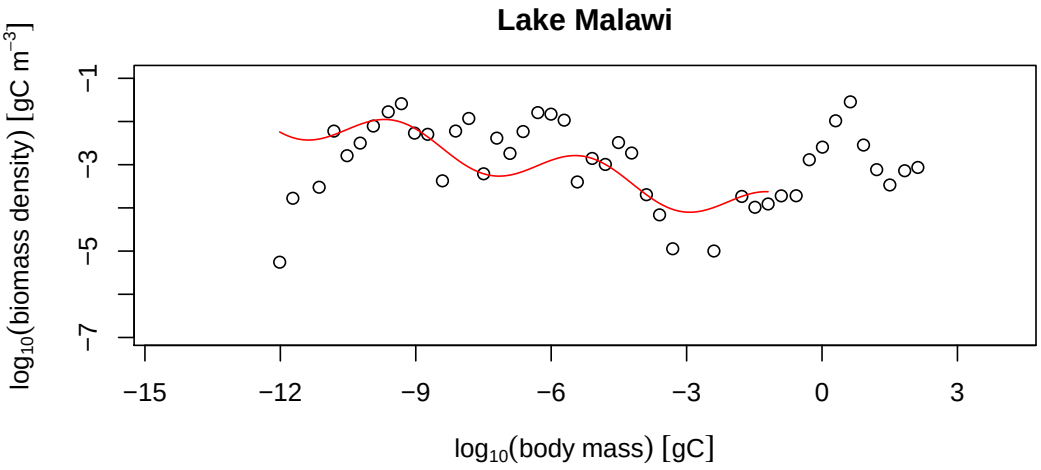
Lake Malawi
log10(biomass density) [gC m−3]
−1
−3
−5
−7
−15
−12
−9
−6
−3
0
3
log10(body mass) [gC]

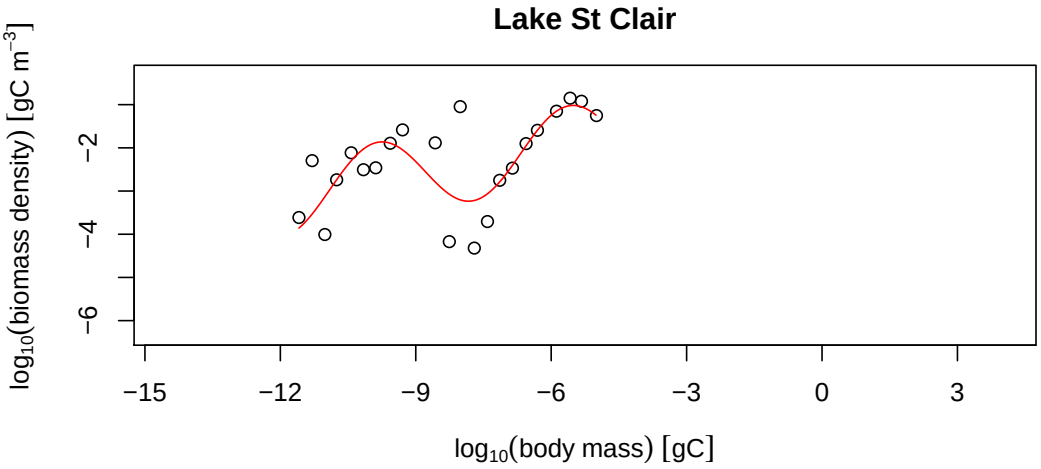
Lake St Clair
log10(biomass density) [gC m−3]
−2
−4
−6
−15
−12
−9
−6
−3
0
3
log10(body mass) [gC]

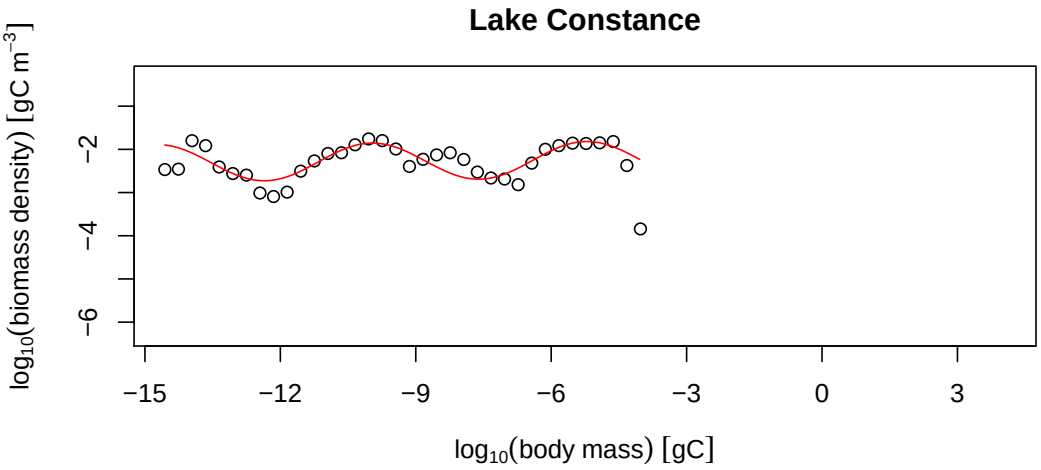
Lake Constance
log10(biomass density) [gC m−3]
−2
−4
−6
−15
−12
−9
−6
−3
0
3
log10(body mass) [gC]

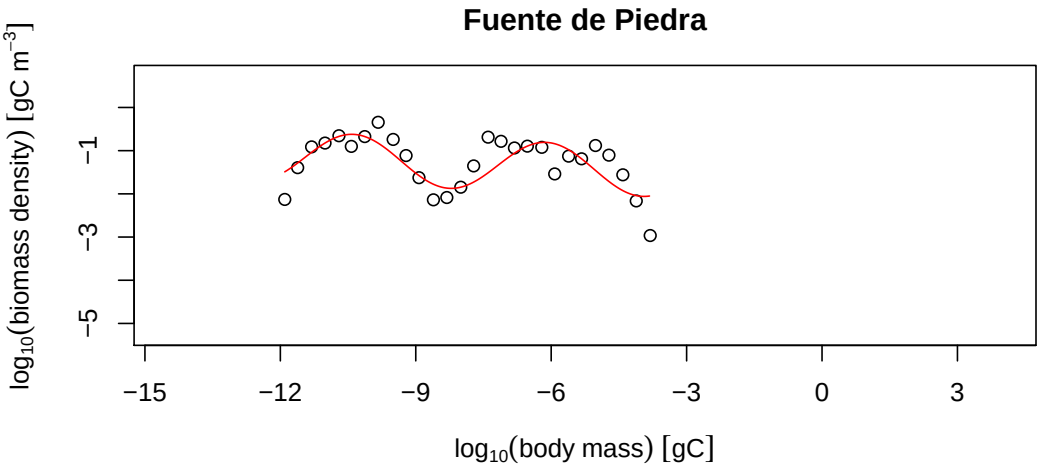
Fuente de Piedra
log10(biomass density) [gC m−3]
−1
−3
−5
−15
−12
−9
−6
−3
0
3
log10(body mass) [gC]

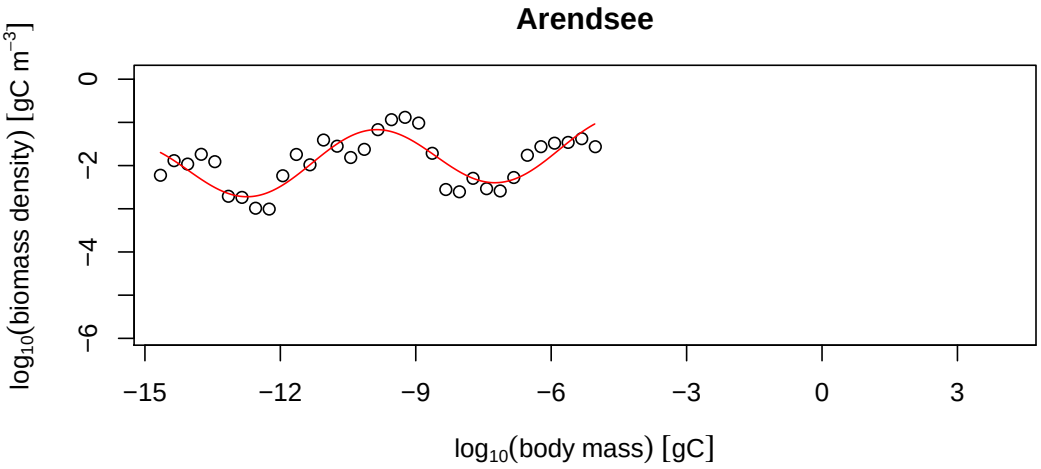
Arendsee
log10(biomass density) [gC m−3]
0
−2
−4
−6
−15
−12
−9
−6
−3
0
3
log10(body mass) [gC]

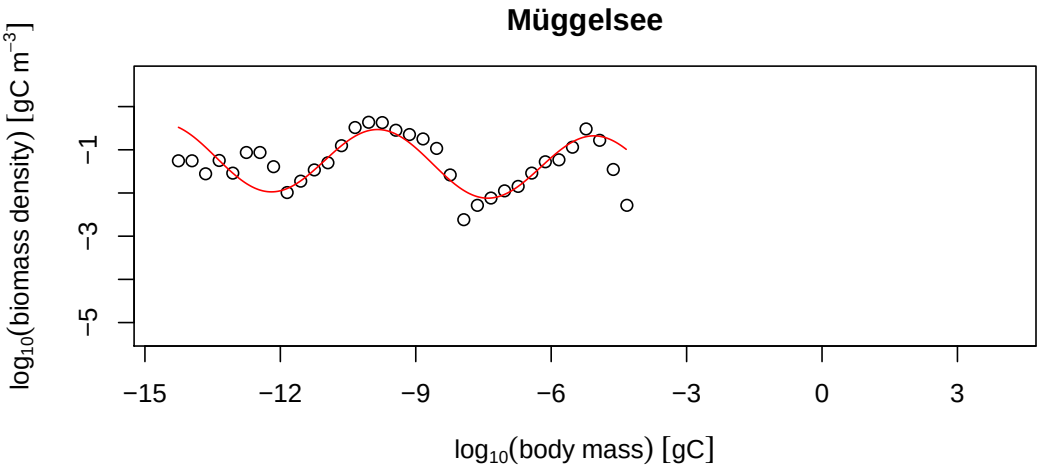
Müggelsee
log10(biomass density) [gC m−3]
−1
−3
−5
−15
−12
−9
−6
−3
0
3
log10(body mass) [gC]

Characteristic	Scale	c_0	c_1	c_1/c_0	p	$\mathrm{corr}(c_0, c_1)$
Intercept B_0	$\log_{10}(\mathrm{gC\,m^{-3}})$	$-4.25(11)$	$1.53(14)$		9.5×10^{-11}	-0.42
Slope S	dimensionless	$-0.1197(71)$	$0.0789(86)$	-0.66	3.5×10^{-09}	-0.4
Amplitude A	$\log_{10}$(biomass)	$0.363(36)$	$0.095(32)$	0.26	0.0068	-0.6
Separation D	$\log_{10}$(body mass)	$5.30(19)$	$-0.34(16)$	-0.064	0.042	-0.81

Supplementary Table 2: For each characteristic $C = B_0$, S, A, D, the table gives details of the weighted linear regression $C = c_0 + c_1 \log_{10}(\mathrm{TP}/\mu\mathrm{g\,L^{-1}})$. Figures in parentheses represent standard errors of regression coefficients, p relates to the null-hypothesis $c_1 = 0$ (two-tailed).

Supplementary Note 5: Regressions of empirical size-spectrum characteristics *vs* nutrient enrichment

In Supplementary Table 2, we provide details of weighted linear regressions of the four empirical size-spectrum characteristics B_0, S, A, and D against $\log_{10}$ TP. Weights were taken as the inverse squared standard errors of data points. The weighted regressions were computed using the lm function of the R programming language [17, version 3.4.2]. The ratio c_1/c_0 is tabulated as a measure of effect strength, excluding the case of B_0 where this value depends on the units of measurement chosen. This shows that the effect of nutrient enrichment on the separation between domes D is weak compared to the effects on slope S and dome amplitude A.

Supplementary Note 6: The linear SSSM and its responses to size-specific pressures

In Supplementary Note 7 below we present an analysis showing that domes in the SSSM are generated by an amplifying top-down cascade resulting from nutrient enrichment. The analysis is carried out using the linearized version of the model described above, the linear SSSM. In the present section the linear SSSM and the linear response theory derived for it in CAT are briefly recalled.

6.1 Formulation of the linear SSSM

Two variants of the linear SSSM have been analysed in CAT. They were there referred to as the "oligotrophic" and the "eutrophic" regime. Here, we consider the oligotrophic regime, defined in Supplementary Note 1 above. In this regime, dynamics are linearized around an idealised equilibrium model state $B(m_*) = B_0(m_*)$ of the form

$$B_0(m_*) = \tilde{B}_{\mathrm{tot}} m_*^{1-\lambda} \quad (\text{for all } m_* > 0), \tag{8}$$

with $\tilde{B}_{\mathrm{tot}}$ given by Eq. (6).

The linear SSSM is best formulated using instead of m_* the logarithmic maturation body mass variable $u = \ln(m_*/M)$, with M denoting some reference body mass, e.g. $1\,\mathrm{gC}$. The distribution of a community's biomass over the u-axis is given by $m_* B(m_*) = M\mathrm{e}^u B(M\mathrm{e}^u)$. We follow CAT and denote by $b(u)$ deviations of this distribution from that given by the base state, that is

$$b(u) = M\mathrm{e}^u B(M\mathrm{e}^u) - M\mathrm{e}^u B_0(M\mathrm{e}^u). \tag{9}$$

The linear SSSM is an integro-differential equation for the dynamics of $b(u)$. Absent any external pressures, they are given by

$$\frac{\partial b(u)}{\partial t} = (M\mathrm{e}^u)^{n-1} \int_{-\infty}^{\infty} \tilde{K}(u-v) b(v) dv. \tag{10}$$

In this equation, the interaction kernel $\tilde{K}(w)$ describes for any $w = u - v$ the strength of the effect of populations of species of size $M\mathrm{e}^v$ on a focal species of size $M\mathrm{e}^u$. The parameter w is thus a logarithmic size ratio $w = \ln[(M\mathrm{e}^u)/(M\mathrm{e}^v)]$. The interaction kernel $\tilde{K}(w)$ incorporates all the "ecology" of the model. In the SSSM, it contains contributions due to predation mortality and density-dependent growth, and a term describing damping due to food-web effects, corresponding to that in Eq. (3) above. An explicit formula will be given in Supplementary Note 7 below. The factor $(M\mathrm{e}^u)^{n-1}$ in Eq. (10) models the size dependence of the time scale of demographic processes: populations of smaller species tend to change faster than those of larger species (note that $n < 1$, Supplementary Table 1).

6.2 Fourier transforms

Below we shall make heavy use of Fourier transforms of continuous functions. Here we specify the particular form in which we define Fourier transforms, because conventions for this vary in the literature. For any function $f(x)$ defined over the real numbers, we define its Fourier transform $\hat{f}(\xi)$ such that, at least formally,

$$\hat{f}(\xi) = \int_{-\infty}^{\infty} \mathrm{e}^{-\mathrm{i}\xi x} f(x)\, dx, \quad f(x) = \int_{-\infty}^{\infty} \frac{\mathrm{e}^{\mathrm{i}\xi x}}{2\pi} \hat{f}(\xi)\, d\xi, \tag{11}$$

where i is the imaginary unit ($\mathrm{i}^2 = -1$) and ξ is a real- or complex-valued variable. For a gentle but mathematically rigorous discussion of Fourier transforms and related topics, see e.g. [18].

6.3 Linear response theory for the SSSM

How will the species size spectrum respond when species *of a specific size* are subjected to a persistent, constant pressure, such as continuous removal, stocking, or feeding, i.e., a press

perturbation? What is the new equilibrium reached after all ecological interactions up and down the size axis have played out? A general analysis of equations of the form (10) suggests that the following recipe answers this question (CAT, Sec. 8.4.3):

1. Compute from $\tilde{K}(w)$ its Fourier transform $\hat{K}(\xi)$.

2. Obtain the analytic continuation of $\hat{K}(\xi)$ into the complex plane (if an explicit expression for $\hat{K}(\xi)$ is available, this usually amounts to simply permitting ξ to attain any complex value, up to a few values where $\hat{K}(\xi)$ might be singular).

3. Find the first few zeros of $\hat{K}(\xi)$ in the complex plane (the values of ξ where $\hat{K}(\xi) = 0$) in order of increasing $|\xi|$, and evaluate the derivatives $\hat{K}'(\xi) = d\hat{K}(\xi)/d\xi$ at these zeros.

4. Draw a graph of the complex plane, indicating in it each zero of $\hat{K}(\xi)$ by an arrow pointing from the zero ξ into the direction $(\,\mathrm{Re}[\hat{K}'(\xi)],\ \mathrm{Im}[\hat{K}'(\xi)]\,)$. Then draw the line $\mathrm{Im}(\xi) = -(2-\lambda) = \lambda - 2$, with λ defined as in Supplementary Table 1. An example of such a graph is given in Supplementary Figure 3. For the representation of size spectra used here, the value $2-\lambda$ corresponds to the slope (actually: power-law exponent) of the ideal power-law size spectrum in the oligotrophic regime.

5. From this graph, read off the responses of the species size spectrum to a press perturbations on a give size class as follows. The zeros come in pairs $\pm\,\mathrm{Re}(\xi) + \mathrm{i}\,\mathrm{Im}(\xi)$, unless $\mathrm{Re}(\xi) = 0$. Each of these pairs or imaginary singletons corresponds to one type of response. If the attached arrow points upwards, it is a top-down response, where species smaller that those perturbed are being affected. If the attached arrow points downward, it is a bottom-up response.

   Purely imaginary zeros correspond to un-modulated size-spectrum responses. In all other cases the response is modulated, i.e. a "cascade". The wavelength of the modulation along the u axis is $|2\pi/\,\mathrm{Re}(\xi)|$. That is, neighbouring maxima (e.g. the domes) occur for species with maturation body sizes differing by an approximate factor $\exp(|2\pi/\,\mathrm{Re}(\xi)|)$.

   If the attached arrow points towards the line $\mathrm{Im}(\xi) = \lambda - 2$, the response is attenuating, i.e. the proportional change in $B(m_*)$ tends to become smaller the more m_* is different from the size of the perturbed species. Conversely, if the attached arrow points away from the line $\mathrm{Im}(\xi) = \lambda - 2$, the response is amplifying, i.e. the proportional change in $B(m_*)$ tends to become larger the more m_* is different from the size of the perturbed species. Quantitatively, the amplitude of the proportional change in $B(m_*)$ for species that are by a factor Z larger or small than those perturbed is by a factor $Z^{|\,\mathrm{Im}(\xi)-\lambda+2|}$ larger or smaller than that of the perturbed species.

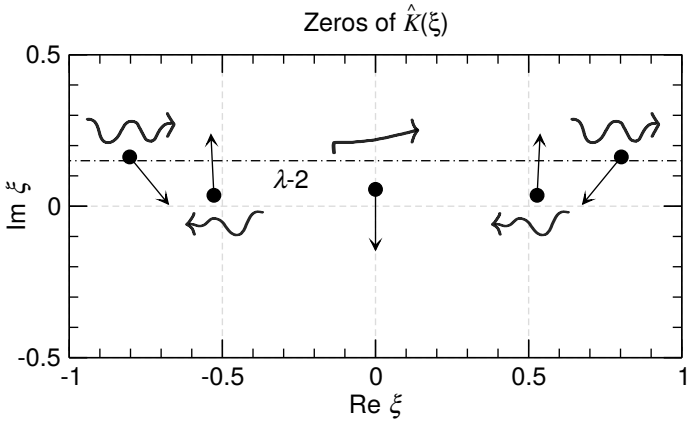

Supplementary Figure 3: Points in the complex plane corresponding to the main responses of the SSSM to press perturbations. Corresponding size-spectrum responses are illustrated. From the centre outwards, these are the conventional bottom-up effect, the conventional top-down cascade, and a bottom-up cascade. Parameters as in Supplementary Table 1 with $x = 1$ (which implies $y = 1$ below).

In Supplementary Figure 3, which corresponds the parameter set used in the main text (Supplementary Table 1) with $x = 1$, one sees, in order of increasing distance from the origin of the complex plane, one imaginary singleton and two complex pairs. These are the three kinds of responses of size spectra to pressures mentioned in the main text:

1. The singleton at $\xi = 0 + 0.055\,\mathrm{i}$ has a downward-pointing arrow attached. It therefore corresponds to an un-modulated bottom-up effect. Because it points away from the dashed-dotted line, the effect is amplifying. This is the conventional bottom-up effect with trophic amplification. [The ecological reason for trophic amplification is that more abundant prey can not only sustain more predators, the prey is also easier to find; see 6, Section 21.2.2.]

2. The pair of zeros at $\xi = \pm 0.528 + 0.034\,\mathrm{i}$ has upward-pointing arrows attached. It therefore corresponds to a modulated top-down effect. Because the arrows point towards the dashed-dotted line, the effect is attenuating. This is the conventional trophic cascade, here with effect strengths declining towards lower trophic levels, as observed for marine pelagic systems [19].

3. The pair at $\xi = \pm 0.803 + 0.163\,\mathrm{i}$ has downward-pointing arrows attached. It therefore corresponds to a modulated bottom-up effect, i.e. a bottom-up cascade as predicted by the classical theory [20, 21, 22]. Because these zeros are (for the chosen parameters) located very close to the line $\mathrm{Im}\,\xi = \lambda - 2 = 0.15$ (cf. Supplementary Table 1), the cascade is

effectively neither amplifying not attenuating. However, with increasing nutrient levels it gets "drowned out" by trophic amplification (see below).

Zeros even farther away from the origin appear to always correspond to attenuating responses (e.g. Supplementary Figure 6). They are less important ecologically, because with increasing $|\operatorname{Re}\xi|$ the corresponding wavelength on the u-axis becomes shorter and with increasing $|\operatorname{Im}\xi|$ attenuation becomes stronger, which makes them relevant only for highly size-specific pressures and only for species of size very similar to those where pressure is applied.

6.4 Demonstration of the recipe on a simple example

The method described above has been verified numerically in CAT. In this section, we demonstrate it for a highly simplified, exactly solvable problem as a transparent illustration of how the method works. We will first introduce the example problem and its exact solution, and then compare this solution with the predictions made in Sec. 6.3 above.

Consider the simple drift-diffusion-growth equation,

$$\frac{df(x,t)}{dt} = rf(x,t) - v\frac{df(x,t)}{dx} + D\frac{d^2f(x,y)}{dx^2}, \tag{12}$$

which specifies how the distribution of some quantify $f(x,t)$ over the x axis how it changes through time t. The three terms on the right-hand-side describe self-reproduction at a rate r, drift along the x axis with velocity v and diffusion at a rate $D > 0$. This equation has, amongst others, solutions of the form of drifting Gaussians

$$f(x,t) = f_{\mathrm{G}}(x,t;f_0,\sigma_0) \stackrel{\text{def}}{=} \frac{f_0 \mathrm{e}^{rt}}{\sqrt{2\pi(2Dt+\sigma_0^2)}} \exp\left[-\frac{(x-vt)^2}{4Dt+2\sigma_0^2}\right], \tag{13}$$

with free parameters f_0 and σ_0. Now, consider a modification of Eq. (12) where for $t \geq 0$ a Gaussian inhomogeneity of width σ centred at $x = 0$, representing a press perturbation, is added to its right-hand side:

$$\frac{df(x,t)}{dt} = rf(x,t) - v\frac{df(x,t)}{dx} + D\frac{d^2f(x,y)}{dx^2} + \frac{\mathrm{e}^{-x^2/(2\sigma^2)}}{\sqrt{2\pi}\sigma} \quad (\text{for } t \geq 0). \tag{14}$$

If one assumes $f(x,t) \equiv 0$ for $t < 0$, this equation has for $t \geq 0$ a unique solution that can be represented by an integral over drifting Gaussians that originated from the inhomogeneity during the times τ between zero and t:

$$f(x,t) = f_{\mathrm{I}}(x,t) \stackrel{\text{def}}{=} \int_0^t f_{\mathrm{G}}(x,t-\tau;1,\sigma)d\tau. \tag{15}$$

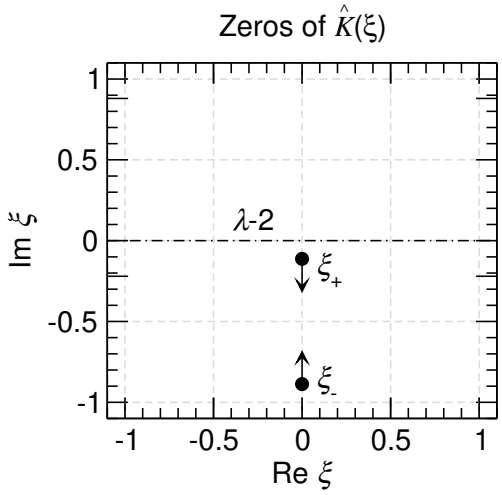

Supplementary Figure 4: The two points in the complex plane corresponding to zeros of the interaction kernel for the simple model of Sec. 6.4. Parameters $v = 1$, $D = 1$, $r = 0.1$. The two zeros are given by Eq. (21); $\lambda = 2$.

In the limit $\sigma \to 0$, this integral evaluates to

$$f_{\mathrm{I}}(x,t) = \frac{\mathrm{e}^{(xv-|x|\sqrt{v^2-4Dr})/(2D)}}{2\sqrt{v^2-4Dr}}\,\mathrm{erfc}\left(\frac{|x|-t\sqrt{v^2-4Dr}}{2\sqrt{Dt}}\right) \quad + \\ \frac{\mathrm{e}^{(xv+|x|\sqrt{v^2-4Dr})/(2D)}}{2\sqrt{v^2-4Dr}}\,\mathrm{erfc}\left(\frac{|x|+t\sqrt{v^2-4Dr}}{2\sqrt{Dt}}\right), \quad (16)$$

with erfc denoting the complementary error function [23]. This solution can be verified directly by inserting it into Eq. (14) and taking the limit $\sigma \to +\infty$. In the following, we concentrate on the case $4Dr < v^2$, where the arguments of the error functions are real-valued. For real arguments y, the function $\mathrm{erfc}(y)$ transitions smoothly from 2 to 0 as y passes from negative to positive values. The first term in Eq. (16) therefore describes two fronts that propagate at a speed $\pm\sqrt{v^2-4Dr}$ away from zero. The first occurrence of erfc in Eq. (16) approaches 2 after sufficiently long waiting times t for any fixed value of x. The second occurrence converges to zero as t increases. The solution therefore reaches the steady state

$$\lim_{t\to+\infty} f_{\mathrm{I}}(x,t) = \frac{\mathrm{e}^{(xv-|x|\sqrt{v^2-4Dr})/(2D)}}{\sqrt{v^2-4Dr}}. \quad (17)$$

We now show that this result is consistent with the recipe of Sec. 6.3 when adapting it to Eq. (12). The equation can be rewritten as

$$\frac{df(x,t)}{dt} = \int_{-\infty}^{+\infty} K(x-y)f(y,t)dy, \tag{18}$$

with an interaction kernel

$$K(x) = r\delta(x) - v\delta'(x) + D\delta''(x), \tag{19}$$

where $\delta(x)$ represents the Dirac delta function. Complications due to deviations from Sheldon's hypothesis [24] ($\lambda \neq 2$) are not relevant here, we therefore set $\lambda = 2$ when applying the recipe.

Step 1 of the recipe is to compute the Fourier transform of $K(x)$. According to Eq. (11) this is

$$\hat{K}(\xi) = r - \mathrm{i}v\xi - D\xi^2. \tag{20}$$

Because $\hat{K}(\xi)$ is an entire function in ξ, its analytic continuation into the complex plane, required by Step 2, is formally identical.

Step 3 requires computation of the zeros of $\hat{K}(\xi)$. As for the direct solution of Eq. (14) above, we concentrate on the case $4Dr < v^2$. Further, we consider only the case $v > 0$; the analysis for $v < 0$ is analogous. Under these conditions, $\hat{K}(\xi)$ has two purely imaginary zeros given by

$$\xi_+ = \frac{-v + \sqrt{v^2 - 4Dr}}{2D}\,\mathrm{i} \qquad \text{and} \qquad \xi_- = \frac{-v - \sqrt{v^2 - 4Dr}}{2D}\,\mathrm{i}, \tag{21}$$

with $|\xi_+| < |\xi_-|$. If r has a value close to zero one can approximate $\xi_+ \approx -\frac{r}{v}\mathrm{i}$ and $\xi_- \approx (-\frac{v}{D} + \frac{r}{v})\mathrm{i}$ to first order in r. That is, ξ_+ then tends to be considerably closer to zero then ξ_- and therefore more important for responses to press perturbations according to the reasoning of Sec. 6.3. At the zeros, the first derivative $\hat{K}'(\xi) = -\mathrm{i}v - 2D\xi$ evaluates to

$$\hat{K}'(\xi_+) = -\sqrt{v^2 - 4Dr}\,i \qquad \text{and} \qquad \hat{K}'(\xi_-) = \sqrt{v^2 - 4Dr}\,i. \tag{22}$$

Figure 4 shows the graph drawn following the instructions of Step 4 for parameters $v = 1$, $D = 1$, $r = 0.1$. Interpreting this graph according to Step 5 *mutatis mutandis*, the arrow for ξ_+ predicts a response that propagates towards larger x (because the arrow points downwards). It is amplifying because it points away from the semi-dashed line (here at $\mathrm{Im}\,\xi = 0$). Correspondingly, the arrow for ξ_- predicts an attenuating response that propagates towards smaller x. Because ξ_- is considerably further away from zero than ξ_+, the decay of the attenuating response is comparatively fast. The corresponding perturbation response therefore does not affect overall system behaviour much.

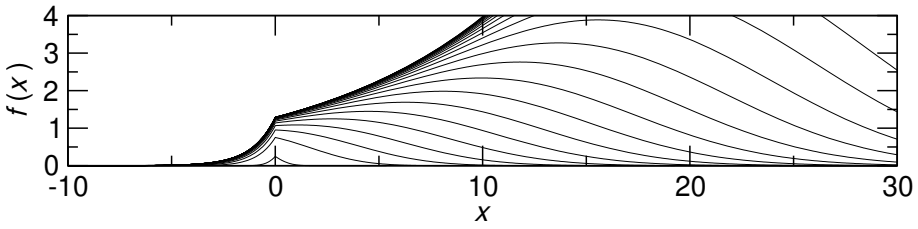

Supplementary Figure 5: Exact solution of Eq. (14) for $\sigma \to 0$, given by Eq. (16), at subsequent points in time starting at $t = 0.2$ and separated by 2 time units. The solution converges to the form given by Eq. (17). Parameters as in Supplementary Figure 4.

In Supplementary Figure 5 the exact solution, Eq. (16), is evaluated for the same set of parameters. As predicted by Eq. (17), it converges to an equilibrium in which $f(x)$ exponentially increases for positive x and exponentially decreases at a faster rate for negative x. Thus all predictions derived from the recipe are borne out: the behaviour of $f(x,t)$ resulting from the press-perturbation at $x = 0$ is dominated by the response amplifying towards larger x, and there is a second response decaying towards smaller x. In passing, we note that a more detailed comparison with results from CAT would show that the method not only predicts the quantitative rates of attenuation and decay along the x axis correctly for this example, but also the speed of propagation of the fronts in Eq. (16) and the denominator in Eq. (17).

From this example problem it is not difficult to construct a corresponding problem with a spatially modulated solution. For any fixed wave number $q > 0$ of the modulation, simply go over to the new dependent variable $g(x,t) = \mathrm{e}^{\mathrm{i}qx} f(x,t)$. Expressed in terms of this new variable, the drift-diffusion-growth equation, Eq. (12), becomes

$$\frac{dg(x,t)}{dt} = rg(x,t) - v\left(\frac{d}{dx} - \mathrm{i}q\right) g(x,t) + D\left(\frac{d}{dx} - \mathrm{i}q\right)^2 g(x,y). \tag{23}$$

The responses of $g(x,t)$ to localised press perturbations, which can be computed directly from those of $f(x,t)$, are modulated patterns with wavelength $2\pi/q$.

It is instructive to compare the approach used here to the linear stability analysis conventionally performed in the study of pattern formation [25]. The conventional approach interprets $\hat{K}(\xi)$ as specifying, for real-valued ξ, the linear growth rate of sinusoidal modulations of $f(x,t)$ with wave number ξ, i.e. wavelength $2\pi/\xi$ [or as a corresponding eigenvalue of the linear operator given by the right-hand-side of Eq. (18)]. The unperturbed system, Eq. (12), is considered stable if $\mathrm{Re}[\hat{K}(\xi)] < 0$ for all real ξ, and unstable if $\mathrm{Re}[\hat{K}(\xi)] > 0$ for some ξ. In our example $\mathrm{Re}[\hat{K}(\xi)] = r - D\xi^2$. The system is therefore linearly stable for $r < 0$ and linearly unstable for $r > 0$ (because then $\mathrm{Re}[\hat{K}(0)] = r > 0$). The transition to instability occurs at $r = 0$, exactly when $\xi_+ \approx -r\mathrm{i}/v$ crosses the real axis, thus signalling the transition from attenuating

to amplifying system responses to localised press perturbations. We have thus shown that, for this example, where both approaches are applicable, the conventional stability analysis and the approach of Sec. 6.3 are equivalent.

A limitation of the method of Sec. 6.3 is that it works by constructing stable steady-state solutions. When responses to pulse perturbations do not drift sufficiently fast to the left or the right on the x axis, responses to press perturbations can pile up at one location and no stable steady-state solutions exist in linear models. Such systems called *absolutely unstable*. By contrast, the instability discussed in the previous paragraph is called a *convective instability*, because of any fix x a steady state is eventually reached. Our simple model, Eq. (12), becomes absolutely unstable for $4Dr \geq v^2$ [26]. Unless $v = 0$, the transition to absolute instability therefore always occurs after the transition to convective instability. This ordering of transitions is generic in extended 1D systems when the symmetry between left and right along the coordinate axis is broken. It permits us here to pin down transitions to convective instability while disregarding complications due to absolute instability.

Supplementary Note 7: Analytic theory for the formation of dome patterns

Mathematically, there are two routes that lead to amplification of top-down cascades with increasing primary production in the non-linear SSSM. The starting point for both is an increase in phytoplankton due to nutrient enrichment, and the resulting conventional, un-modulated bottom-up effect. Because this effect is amplifying towards larger body sizes, it does not only lead to an overall increase in community biomass (Figs. 1a and 3a of the main text), but also makes the fitted slope S of the size spectrum less steep (Fig. 3b). The response of the size spectrum modulation to these changes is a second-order phenomenon: it is a change in how the system responds to pressures resulting from other changes in the system. A rigorous analytic study of this phenomenon would require an extension of the linear SSSM by terms quadratic in $b(u)$, to be derived from the non-linear SSSM; and then a mathematical analysis of this model. Here a simpler, heuristic approach is chosen, where the two effects are described by modifying the formal description of the base state of the linear model itself, followed by an analysis of the consequences that these modifications have for linear responses.

7.1 Implications of a changing size-spectrum slope

The increase in the fitted slope S seen in simulations (Fig. 3b of the main text) is due to trophic amplification of bottom-up effects. In the linear theory, it is represented by the imaginary singleton zero of $\hat{K}(\xi)$ in Supplementary Figure 3. Mathematically, one expects that trophic amplification leads to small deviations of size spectra form a power-law form (CAT, Section 9.6). However, for the semi-quantitative considerations here it is fair to disregard this and

equate the fitted size-spectrum slope S with a modified power-law exponent $2-\lambda$. By the same amount by which S increases in Fig. 3b, the dash-dotted line in Supplementary Figure 3 therefore effectively sinks. Applying the recipe given above for the interpretation this kind of graph to a situation where the dash-dotted line sinks as nutrients increase, one concludes that with increasing nutrient supply bottom-up cascades become (more) attenuating, top-down cascades become less attenuating and conventional bottom-up effects less amplifying.

The ecological interpretation of this is straightforward. An increase in $S \approx 2-\lambda$ means that, in comparison with the biomass of smaller species, the biomass of larger species increases. The effects of responses to pressures that propagate to larger species are therefore attenuated in relative terms. Their effects get "drowned-out" in the high overall biomass of large species. Likewise, the attenuation of the top-down cascade becomes weaker because, if large species are relatively more abundant, changes in their biomass by a small proportion can lead to more pronounced proportional changes in the abundances of smaller species.

The amplification of top-down effects through an increase of the size-spectrum slope S is thus more a matter of book-keeping than of actual ecology, which results from considering relative rather than absolute changes in abundance in empirical data. Nevertheless it is important, because for practical reasons ecologists prefer to compare relative rather than absolute changes [19].

7.2 Implications of overall biomass increase

To understand the effect of an overall increase in community biomass on size-spectrum dynamics, a closer look at the interaction kernel $\tilde{K}(w)$ is required. In CAT (Eqs. [81], [86]), an explicit expression for $\tilde{K}(w)$ was derived in terms of its Fourier transform. With the minor modifications of the SSSM introduced in Supplementary Note 1 above, it reads

$$\hat{K}(\xi) = \tilde{B}_{\text{tot}}\hat{\kappa}_0(\xi+\nu\text{i})\,\hat{\beta}(-\xi-\nu\text{i})\hat{\beta}(\xi) + \overbrace{\hat{X}(\xi)}^{\text{Food-Web}}, \tag{24}$$

where (for the oligotrophic regime) $\nu = 1-q$; the function $\hat{\kappa}_0$ describes individual-level interactions and is given by

$$\hat{\kappa}_0(\xi+\nu\text{i}) = \overbrace{\frac{\alpha h^2 y\gamma}{(y\gamma\tilde{\phi}+h)^2}\hat{s}(\xi)}^{\text{Feeding}} - \overbrace{\frac{y\gamma h}{y\gamma\tilde{\phi}+h}\hat{s}(-\xi-\nu\text{i})}^{\text{Predation}} + \overbrace{\frac{y^2\gamma^2\tilde{\mathcal{N}}h}{(y\gamma\tilde{\phi}+h)^2}\hat{s}(\xi)\hat{s}(-\xi-\nu\text{i})}^{\text{Release}}; \tag{25}$$

$\hat{\beta}(\xi)$ is the Fourier transform of the population structure $\tilde{\beta}(u)$ given by Eq. (7) above, with the two factors in Eq. (24) representing the computation of the individual-based community size spectrum $\mathcal{N}(m)$ from the species size spectrum $B(m_*)$ (Supplementary Table 1) and the computation of species-level dynamics from individual-level interactions (Eq. (1)); and

$$\hat{X}(\xi) = \rho \left[\exp\left(-\frac{\sigma_r^2 \xi^2}{2} \right) - \exp\left(\frac{\sigma_r^2 (\lambda - 2)^2}{2} \right) \right]. \tag{26}$$

This last term describes the damping of short wavelength (i.e. large $|\operatorname{Re}\xi|$) modulations of the size spectrum due to food-web effects. It differs from the form used in CAT by having the constant $\exp\left(\sigma_r^2(\lambda-2)^2/2\right)$ ($= 1.003$ for parameters as in Supplementary Table 1) in place of 1.

The new parameter y in Eq. (25) equals $y = 1$ for the linear SSSM (but see below); $\tilde{\mathcal{N}}$ is the coefficient scaling the community size spectrum of the base state; $\tilde{\phi} = \tilde{\mathcal{N}}\, \hat{s}\big(i(\lambda-2)\big)$ scales food availability; and $\hat{s}(\xi)$ is the Fourier transform (on a logarithmic scale) of the predator-prey mass-ratio window $s(x)$. For our choice of $s(x)$ (Supplementary Table 1), this is

$$\hat{s}(\xi) = (2\pi)^{1/2} \sigma_s \exp\left[-\frac{\sigma_s^2 \xi^2}{2} \right] \beta^{-\mathrm{i}\xi}. \tag{27}$$

The three named terms in Eq. (25) correspond to different ecological effects. From the derivation of these terms in CAT (Sec. 6.3), one see that *Feeding* describes increases in population growth with increasing density of food; *Predation* describes population decline with increasing density of predators; and the last term, *Release*, describes release from predation in situations where consumers of the focal species are (partially) satiated [27]. The focal size class then experiences a safety-in-numbers effect that reduces its *per capita* predation mortality. This release from predation increases as the focal size class and species of similar size become more abundant, and *vice versa*.

We included a factor y in several places in Eq. (25) as a simple way to model the effects of an overall increase of community biomass in the SSSM. Values $y \neq 1$ describe the effects of scaling the biomass of the based state by a factor y, which formally results from multiplying $\tilde{B}_{\text{tot}}$ by y. This includes the direct effect *via* Eq. (25), and indirect effects through the scale factors for community size spectrum $\tilde{\mathcal{N}}$ and food availability $\tilde{\phi}$. Alternatively and perhaps more transparently, $y \neq 1$ can be interpreted as describing effective re-scaling of the value of the coefficient of search&attack rates γ: every occurrence of γ in Eq. (25) goes along with a factor y.

Important for the following is that changes in y affect the magnitude of the three named terms in $\hat{\kappa}_0$ in different ways. For y smaller than $h/\gamma\tilde{\phi}$, the main effect of increasing y is to enhancing the role of the term named Release compared the terms Feeding and Predation, because y enters quadratically in the numerator of Release but only linearly in the numerators of Feeding and Predation. This makes ecological sense, because Release describes an effect resulting from (partial) saturation of consumers. At low food abundance it plays no important role.

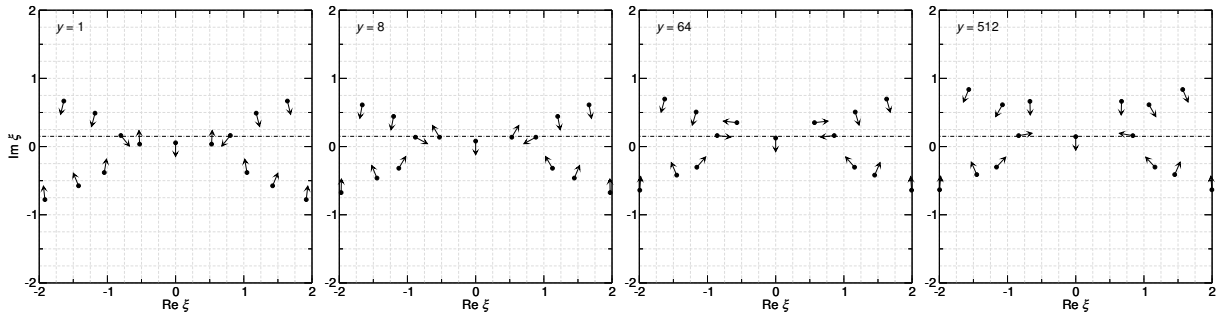

Supplementary Figure 6: Location of the zeros of $\hat{K}(\xi)$ in the complex plane and arrows indicating $\arg d\hat{K}(\xi)/d\xi$ for increasing enrichment y. For $y \approx 8$ the pair of zeros corresponding to top-down cascades crosses the dash-dotted line, signifying a transition from attenuating to amplifying top-down cascades.

However, as y increases in magnitude beyond $h/\gamma\tilde{\phi}$ and the expression $y\gamma\tilde{\phi} + h$ in the denominators in Eq. (25) can be approximated as $y\gamma\tilde{\phi}$, further increases in y lead to a decline of the importance of Feeding (which then scales as $1/y$) relative to the terms Predation and Release (where y effectively cancels out). Ecologically, this is the transition from density-dependent feeding at low food abundance to effectively density-independent feeding when food is plenty. Supporting this analysis, the expression for $\hat{\kappa}_0$ derived in CAT for the so-called eutrophic regime is identical to that obtained by taking the limit $y \to +\infty$ in Eq. (25).

With this preparation, it is now possible to study mathematically the effects of biomass scaling on how responses to press perturbation propagate along the size spectrum. All one needs to do is to see how the zeros of $\hat{K}(\xi)$ in the complex plane respond to changes in y. For the parameters used here (Supplementary Table 1), this is shown in Supplementary Figure 6.

Interestingly, the strongest response to changes in y in Supplementary Figure 6 is that of the pair of zeros corresponding to the top-down cascade. It moves upward ($\mathrm{Im}\,\xi$ increases) and crosses the line $\mathrm{Im}\,\xi = \lambda - 2$ at about $y = 8$. After crossing the line, the arrows attached to the zeros point away from the line, which means that, by to the rules explained above, the top-down cascade has become amplifying!

With further increases in y, the pair of zeros climbs further, signifying stronger amplification in the linear model (in the full model, non-linear effects set limits to this amplification), until about $y = 64$, where the arrows reverse orientation. Remarkably, biomass scaling has a much weaker effect on the positions of the other zeros, in particular those corresponding to bottom-up cascades.

Figure 6 thus demonstrates that, with the parameters used here, the linear SSSM predicts a transition from attenuating to amplifying top-down cascades when overall community biomass increases. The analytic formulation of the SSSM now allows us to answer in addition the

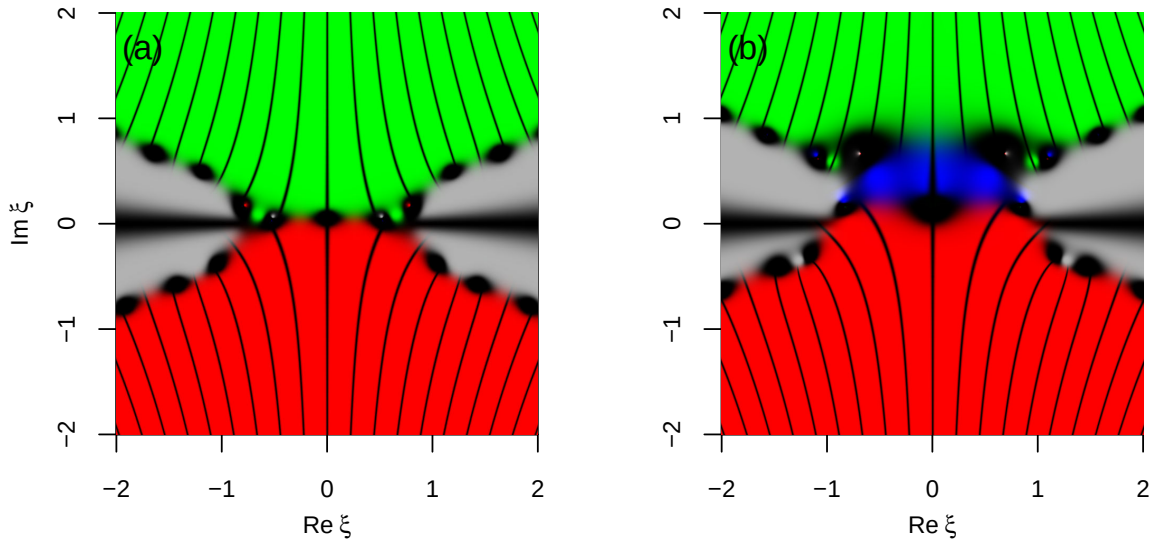

Supplementary Figure 7: Areas of dominance of terms contributing to $\hat{K}(\xi)$ (Eq. (24)) in the complex ξ-plane for (a) $y = 1$ and (b) $y = 512$. Colouring is green for Feeding, red for Predation, blue for Release, and grey for the Food-Web term. For each term $\mathrm{Term}(\xi)$, black lines indicate where the imaginary part of $\mathrm{Term}(\xi)$ is close to zero, thus providing information about how $\arg \mathrm{Term}(\xi)$ changes through the complex plane. The plots were generated by setting the colour intensity for each term to (colour intensity) $= \exp[-7\,|1 - \mathrm{Term}(\xi)/\hat{K}(\xi)|^3]\{1 - [\cos \arg \mathrm{Term}(\xi)]^{100}\}$ and adding intensities. The small coloured spots in both panels are artefacts of this method.

following two questions: what is the underlying mechanism and how generic is it?

The key to addressing these two questions is the observation that in different parts of the complex plane, i.e. depending on ξ, the function $\hat{K}(\xi)$ is dominated by different terms (in the sense that contributions by all other terms are comparatively small). Figure 7a indicates by different colours the areas dominated by the three terms Feeding, Predation (both times the factor $\tilde{B}_{\mathrm{tot}}\hat{\beta}(-\xi - \nu\mathrm{i})\hat{\beta}(\xi)$ from Eq. (24)), and Food-Web for $y = 1$. Their relative positions follow from generic considerations and the formula for Fourier transforms, Eq. (11), with complex argument: Feeding dominates in the upper complex plane because it describes predominantly the dependence on smaller (food) species; Predation dominates in the lower complex plane because it describes the impacts of larger species; and Food-Web dominates towards the left and the right along the real axis because all other terms decline to zero in this direction (they must when the predator-prey size ratio window is continuous and bounded) while Food-Web contains a constant contribution (here $\rho \exp(-\sigma_r^2(\lambda - 2)^2/2)$), which describes reduced competition amongst species of very similar size but with otherwise different trophic roles, as explained in Supple-

mentary Note 1 above.

Except for the possibility of zeros due to the $\hat{\beta}$ factors in Eq. (24), which plays no role here, zeros of $\hat{K}(\xi)$ will typically arise only when two or more of the four terms Feeding, Predation, Release, and Food-Web cancel each other. A simple example illustrating this principles is the function $\sin(\xi) = 0.5\exp(\mathrm{i}\xi) - 0.5\exp(-\mathrm{i}\xi)$ for complex-valued arguments ξ. The term $0.5\exp(\mathrm{i}\xi)$ dominates $\sin(\xi)$ in the lower half plane, and $0.5\exp(-\mathrm{i}\xi)$ dominates in the upper half plane. Because $\exp(\mathrm{i}\xi)$ itself has no zeros in the complex plane, $\sin(\xi) = 0$ requires that the two contributions have the same magnitude (specifically, the same absolute value) and cancel each other. This is the case only along the real axis. In addition, for a zero to occur, $\arg[\exp(\mathrm{i}\xi)]$ and $\arg[\exp(-\mathrm{i}\xi)]$ must be identical. Indeed, this happens at certain points along the real axis, because $\arg[\exp(\mathrm{i}\xi)]$ and $\arg[\exp(-\mathrm{i}\xi)]$ depend differently on $\mathrm{Re}\,\xi$. This is why the zeros of $\sin(\xi)$ are lined up along the real axis. By the same reasoning, the zeros of $\hat{K}(\xi)$ will generally line the boundaries between areas of dominance of terms, where contributions from different ecological effects balance each other.

These considerations, combined with Supplementary Figure 7a, explain the positions of the zeros in Supplementary Figures 3 and 6 for $y = 1$. Specifically, the zeros corresponding to the conventional bottom-up and top-down effects result essentially form a balance of Feeding and Predation. The zero corresponding to the bottom-up cascade is already strongly affected by the Food-Web term; without food-web effects, the resulting perturbation response would be more strongly amplifying. All other zeros, representing strongly damped cascades, result from either a direct balance between Food-Web and Feeding or between Food-Web and Predation.

To understand why the conventional top-down effect responds particularly sensitively to biomass scaling, as illustrated in Supplementary Figure 6, it is useful to consider first the situation for the very high scaling factor $y = 512$. The dominance of terms in the complex plane for $y = 512$ is shown in Supplementary Figure 7b. As for $y = 1$, generic considerations are sufficient to understand the relative positions of areas of dominance. Predation dominates over Release in the lower complex plane, because Predation describes predominantly the impacts of larger species, while Release describes effective interactions amongst species of similar size. Release gradually replaces Feeding with increasing y because of the dependencies of these terms on y discussed above. However, higher up in the complex plane Feeding holds out longer with increasing y because it describes dependence on smaller species, rather than on species of similar size. Finally, dominance of Release develops first in areas with small $\mathrm{Re}\,\xi$ because this effect, involving a chain of two predator-prey interactions (prey-predator-prey), is less size specific than Feeding and Predation. It therefore contributes over a wider range in w to $\tilde{K}(w)$ and, as result, over a narrow range in $\mathrm{Re}\,\xi$ to $\hat{K}(\xi)$. Mathematically in Eq. (25), this narrow range results from the additional factor $\hat{s}(-\xi - \nu\mathrm{i})$ compared to Feeding, which is localised near $\mathrm{Re}\,\xi = 0$.

As Release, with increasing y, breaks up the boundary between the areas dominated by Feeding and Predation, the purely imaginary zero corresponding to the conventional bottom-up effect gets located on the boundary between Release and Predation, while the pair of zeros corresponding to the conventional top-down effect moves along with the boundary between Release and Feeding (Supplementary Figure 7). This, too, can be understood from generic considerations.

The imaginary singleton cannot be located between Release and Feeding, because the two terms have the same sign and cannot compensate each other for un-modulated perturbation responses (i.e. $\mathrm{Re}\,\xi = 0$). The balance must largely be between (positive) Release and (negative) Predation.

For the pair of zeros corresponding to the conventional top-down effect, the situation is opposite. Consider first a population located in a trough of a dome pattern for $y = 1$. The population's size is in equilibrium despite being comparatively low because of a balance of gains (Feeding term) by enhanced food availability from the dome where species are by an approximate factor β smaller and losses (Predation term) due to predation from the dome with species that are approximately β times larger (for focal species located in domes the effects are opposite). This balance is mathematically represented by the corresponding zero in the complex plane.

With $y = 512$, species in troughs experience strong additional losses due to comparatively low predation release (Release term). These losses cannot be compensated by additional losses from predation, only by gains from feeding. Hence Feeding and Release terms must balance in this case and the corresponding pair of zeros be located in the complex plane on the boundary between the areas dominated by these two terms. The pair of zeros therefore moves upward into the complex plane as the area of dominance of Release expands with increasing y.

Even before Release attains a dominating role, it skews the balance between Feeding and Predation in such a way that, with increasing y, the pair of zeros representing the conventional top-down cascade gradually moves upward in the complex plane. Correspondingly, top-down cascades in size spectra gradually become less attenuating with enrichment. Eventually, they become amplifying. *This is the explanation of the amplification of top-down cascades resulting from an overall increase in community biomass.* Based on this explanation, the phenomenon can be expected to be generic: model details did not play a role in explaining it. There is no corresponding mechanism leading to amplification of bottom-up cascades with enrichment.

In the specific case of our model, a comparison of the Feeding and Release terms in Eq. (25) shows that whenever $\arg \hat{s}(-\xi - \nu\mathrm{i}) = \pm\pi$ the arguments of the two terms differ by $\pm\pi$, implying that they can cancel each other. Using Eq. (27), this evaluates to a condition

$$\mathrm{Re}\,\xi = \pm\frac{\pi}{\ln\beta - \sigma_s^2\,(\nu + \mathrm{Im}\,\xi)}. \tag{28}$$

The top-down response becomes amplifying when the corresponding zeros cross the line $\mathrm{Im}\,\xi = \lambda - 2$ (disregarding changes in the size-spectrum slope). Putting this into Eq. (28) and making use of $\nu = 1 - q$ and $\lambda = 2 + q - n$, one can approximate the maturation body mass ratio separating successive local maxima of the resulting size-spectrum modulation as

$$\exp\left(\left|\frac{2\pi}{\mathrm{Re}\,\xi}\right|\right) = \beta^2 \exp[-2\,\sigma_s^2\,(1-n)]. \tag{29}$$

With parameters as in Supplementary Table 1, this evaluates to $81163 \approx 10^{4.9}$. Equation (29) thus provides a good approximation of the distance between domes seen in simulations of the non-linear SSSM, reported to be in the range 10^4 to 10^5 in Fig. 3d of the main text. This agreement further confirms the validity of the analytic theory.

It is noteworthy that, as see from Supplementary Figure 7, both the zero corresponding to the conventional bottom-up effect and the zeros corresponding to the top-down cascade are determined by the balance between the three terms Feeding, Predation, and Release in the expression for $\hat{\kappa}_0$ given by Eq. (25). That is, the relevant zeros of $\hat{K}(\xi)$ are well approximated the by zeros of $\hat{\kappa}_0(\xi + \nu\mathrm{i})$. But the function $\hat{\kappa}_0$ describes exclusively individual-level phenomena without regard to species ID—the life history parameters x_0 and η do not enter it. An implication of this observation is that details of life-history are unlikely to play an important role in dome formation.

7.3 Changes in the direction of propagation of trophic cascades in the linear SSSM

In this section, we briefly consider a questions that arise from the analytic theory above and must be addressed for completeness: What is the ecological meaning of the change in orientation at large y of the arrows in Supplementary Figure 6 for the pair of the zeros corresponding to top-down cascades?

In the linear SSSM, modified by inclusion of the parameter y in Eq. (25), the rise in the complex plane with increasing y of the pair of zeros of $\hat{K}(\xi)$ corresponding to top-down cascades is accompanied by a slow rotation of the attached arrow (Supplementary Figure 6). At $y \approx 64$ the arrow turns to point down, rather up, towards the line $\mathrm{Im}\,\xi = \lambda - 2$. The linear theory predicts that in this case perturbation responses will propagate towards species larger than those perturbed and attenuate with larger size ratios.

In principle, this is ecologically plausible. Above it was explained that, for large y, this pair of zeros results from a balance between Feeding and Release. Considering that neither term describes an effect resulting from species that are much larger than the focal species (as Predation does), but the Feeding term depends on smaller species, a propagation of the perturbation response towards larger species can be expected. Attenuation of this bottom-up response is a plausible expectation, because, for nearly satiated consumers, changes in the abundance of the

prey of a focal size class have only little effect on Feeding, so that only small changes in the abundance of the focal size class are required to compensated this through Release (i.e. release from even higher predation). From these considerations, one would hence expect dome patterns to disappear with strong enrichment.

In simulations of the non-linear SSSM, however, this is not observed (Fig. 3c of the main text). The reason is probably that, with large eutrophication parameter y, system states differ too much from the underlying base state to approximate their dynamics by the linear SSSM. For example, troughs in species size spectra of highly eutrophic systems might be so deep that species with sizes located within domes experience food limitation, despite the high overall abundance of biomass. This would undermine the chain of reasoning above. In situations as the present, where non-linear and linear SSSM disagree in their predictions, the full, non-linear model should be considered the more reliable. The expectation that domes might disappear with strong enrichment thus seems to be an artefact of the linearization.

7.4 Conclusions

This concludes our mathematical analysis of the mechanisms leading to dome formation in the SSSM. Enrichment can transform attenuating top-down cascades into amplifying cascades by two mechanisms. Firstly, through an increase of the fitted size-spectrum slope S, which implies a sinking of the dash-dotted line in Supplementary Figure 3. This mechanism has the opposite (damping) effect on bottom-up cascades. Secondly, enrichment amplifies top-down cascades by an overall increase in community biomass, which lets the pair of zeros corresponding to top-down cascades in Supplementary Figure 3 rise. The latter is caused by (partial) satiation of predators, which reduces their ability to control the abundance of their prey because (1) their feeding rate becomes less dependent on prey abundance and (2) the prey of satiated consumers experiences a safety-in-numbers effect [27]. Equilibrium prey abundances therefore respond stronger to changes in predator abundance, which enhances top-down cascades. (There is no corresponding effect for bottom-up cascades.)

With a sinking dash-dotted line and a rising pair of zeros for top-down cascades, the two will eventually cross, signalling the transition to amplifying top-down cascades. While our analytic approach is too coarse to compute for exactly what value of enrichment x this will happen, we can give an upper bound. For any value of $x > 1$, the resulting increase in overall biomass is at least x-fold (in fact, it is larger because of trophic amplification). For $x > 8$, the corresponding value of y must therefore be > 8 as well. But for any y just slightly larger than 8 the relevant pair of zeros will have crossed the dash-dotted line (Supplementary Figure 6), especially if that line has sunken below the base-state level. Hence, amplifying top-down cascades arise in the non-linear SSSM at some value of x between 1 and 8. This is the range within which dome formation is seen in simulations. We conclude that amplification of top-down cascades with

enrichment is causing dome formation. The conclusion is supported by the observation that the mass ratio separating consecutive domes in the nonlinear SSSM (10^D, with D as in Fig. 3d) is numerically close to the predicted mass ratio separating the maxima of top-down cascades at the onset of amplification, given by Eq. (29).

Supplementary References

[1] Rossberg AG (2012) A complete analytic theory for structure and dynamics of populations and communities spanning wide ranges in body size. *Adv. Ecol. Res.* 46:429–522.

[2] Hartvig M, Andersen KH, Beyer JE (2011) Food web framework for size-structured populations. *J. Theor. Biol.* 272(1):113–122.

[3] Rossberg AG, Farnsworth KD (2011) Simplification of structured population dynamics in complex ecological communities. *Theor. Ecol.* 4(4):449–465.

[4] Fisher RA (1930) *The Genetical Theory of Natural Selection*. (Oxford University Press, Oxford).

[5] van den Bosch F, Metz JAJ, Diekmann O (1990) The velocity of spatial population expansion. *J. Math. Biol.* 28(5):529–565.

[6] Rossberg AG (2013) *Food Webs and Biodiversity: Foundations, Models, Data*. (Wiley).

[7] Naisbit RE, Rohr RP, Rossberg AG, Kehrli P, Bersier LF (2012) Phylogeny versus body size as determinants of food-web structure. *Proc. R. Soc. B* 279(1741):3291–3297.

[8] Kiørboe T, Hirst AG (2014) Shifts in mass scaling of respiration, feeding, and growth rates across life-form transitions in marine pelagic organisms. *Am. Nat.* 183(4):E118–E130.

[9] Barnes C, Maxwell D, Reuman DC, Jennings S (2010) Global patterns in predator-prey size relationships reveal size dependency of trophic transfer efficiency. *Ecology* 91(1):222–232.

[10] Hansen B, Bjornsen PK, Hansen PJ (1994) The size ratio between planktonic predators and their prey. *Limnol. Oceanogr.* 39(2):395–403.

[11] Lampert W (1987) Laboratory studies on zooplankton-cyanobacteria interactions. *N. Z. J. Mar. Freshw. Res.* 21(3):483–490.

[12] Rodriguez J, Mullin MM (1986) Relation between biomass and body weight of plankton in a steady state oceanic ecosystem. *Limnol. Oceanogr.* 31:361–370.

[13] Quiñones RA, Platt T, Rodriguez J (2003) Patterns of biomass-size spectra from oligotrophic waters of the Northwest Atlantic. *Prog. Oceanogr.* 57:405–427.

[14] Rossberg AG, Farnsworth KD, Satoh K, Pinnegar JK (2011) Universal power-law diet partitioning by marine fish and squid with surprising stability-diversity implications. *Proceeding R. Soc. B* 278(1712):1617–1625.

[15] Hendriks AJ, Mulder C (2008) Scaling of offspring number and mass to plant and animal size: Model and meta-analysis. *Oecologia* 155(4):705–716.

[16] Hindmarsh AC, et al. (2005) SUNDIALS: Suite of nonlinear and differential/algebraic equation solvers. *ACM Trans Math Soft* 31(3):363–396.

[17] R Core Team (2017) *R: A Language and Environment for Statistical Computing*. (R Foundation for Statistical Computing, Vienna, Austria).

[18] Boccara N (1990) *Functional Analysis: An Introduction for Physicists*. (Academic Press, New York).

[19] Shurin JB, et al. (2002) A cross-ecosystem comparison of the strength of trophic cascades. *Ecol. Lett.* 5(6):785–791.

[20] Boudreau PR, Dickie LM, Kerr SR (1991) Body-size spectra of production and biomass as system-level indicators of ecological dynamics. *J. Theor. Biol.* 152(3):329–339.

[21] Thiebaux ML, Dickie LM (1992) Models of aquatic biomass size spectra and the common structure of their solutions. *J. Theor. Biol.* 159(2):147–161.

[22] Thiebaux ML, Dickie LM (1993) Structure of the body-size spectrum of the biomass in aquatic ecosystems: A consequence of allometry in predator-prey interactions. *Can. J. Fish. Aquat. Sci.* 50:1308–1317.

[23] Abramowitz M, Stegun IA, eds. (1972) *Handbook of Mathematical Functions*. (Dover, New York).

[24] Sheldon RW, Prakash A, Sutcliffe, Jr. WH (1972) The size distribution of particles in the ocean. *Limnol. Oceanogr.* 17:327–340.

[25] Cross MC, Hohenberg PC (1993) Pattern formation outside of equilibrium. *Rev Mod Phys* 65:851.

[26] Cross MC (1988) Structure of nonlinear traveling-wave states in finite geometries. *Phys. Rev. A* 38(7):3593–3600.

[27] Karban R (1982) Increased reproductive success at high densities and predator satiation for periodical cicadas. *Ecology* 63(2):321–328.